

# Vibrational tunneling spectra of molecules with asymmetric wells: a combined vibrational configuration interaction and instanton approach

Mihael Eraković<sup>1</sup> and Marko T. Cvitaš<sup>1, a)</sup>

*Department of Physical Chemistry, Ruđer Bošković Institute, Bijenička Cesta 54, 10000 Zagreb, Croatia*

(Dated: 19 January 2022)

A combined approach that uses the vibrational self-consistent field (VSCF) and vibrational configuration interaction (VCI) method together with the semiclassical instanton theory was developed to study vibrational tunneling spectra of molecules with multiple wells. The method can be applied to calculate low-lying vibrational states in the systems with arbitrary number of wells, which are not necessarily related by a symmetry operation. It is particularly suited to systems in which the wells are separated by large potential barriers and tunneling splittings are small, so that the exact quantum-mechanical methods come at a prohibitive computational cost. The accuracy of the method was tested on a two-dimensional double-well model system and on malonaldehyde, and the results were compared with the exact quantum-mechanical calculations. The method was subsequently applied to the asymmetrically deuterated malonaldehyde, which has non-degenerate vibrational frequencies in the two wells. The spectrum is obtained at a cost of single-well VSFC/VCI calculations. The interactions between states of different wells are computed semiclassically at a comparatively negligible computational cost. The method is particularly suited to the computation and assignment of spectra in the studies of water clusters.

## I. INTRODUCTION

Physical systems with multiple energetically stable minima are ubiquitous in chemistry and physics<sup>1</sup>. Bound states that are localized in such wells, separated by potential barriers, interact via quantum tunneling, which results in observable shifts of their energies<sup>2,3</sup>. For equivalent, symmetry-related wells, the states that would be degenerate in the absence of tunneling, produce a splitting pattern of energy levels.

Molecules and molecular complexes with two or more equivalent stable configurations are multidimensional systems that display these effects in their vibrational spectrum. The inversion of ammonia<sup>4</sup>, proton tunneling in malonaldehyde<sup>5</sup>, double proton transfer in porphycene<sup>6</sup> or bond rotation in vinyl radical<sup>7</sup> are examples of symmetric double-well systems that produce measurable tunneling splittings (TS) of their vibrational state energies. Water clusters are prototype multiwell systems that exhibit nontrivial splitting patterns caused by tunneling rearrangements between many stable configurations of the cluster<sup>8</sup>.

The asymmetric systems, which have non-equivalent wells, have been less studied. When the state energies of different wells are in resonance, the tunneling dynamics will again cause the delocalization of the wavefunction across the wells and the energy shifts in the spectrum<sup>3</sup>. Away from the resonance, the states remain localized in one well. The asymmetry can be induced in symmetric molecular systems by asymmetric isotopic substitutions<sup>9</sup>. The normal modes and vibrational frequencies in equivalent symmetry-related potential wells then differ and the

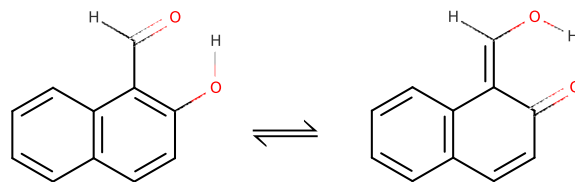


FIG. 1. Tunneling tautomers of 2-hydroxy-1-naphthaldehyde.

correspondence of the vibrational wavefunctions of different wells is not preserved in general. As an example, the malonaldehyde molecule deuterated at D7/D9 position (see Figure 3) thus has an asymmetric level structure with the localized states and those that are delocalized across the multiple minima<sup>9</sup>. A mixing angle between the left-right ground vibrational states of partially deuterated malonaldehyde has experimentally been determined in Ref. 10. Further examples of the mixing have been studied in HF-HD dimer<sup>11</sup> and partially deuterated vinyl radical<sup>12</sup>, CHD-CH, using full-dimensional exact calculations. The splitting pattern in partially deuterated water trimers HDO(H<sub>2</sub>O)<sub>2</sub> and D<sub>2</sub>O(H<sub>2</sub>O)<sub>2</sub> have been determined in experiment<sup>13</sup> and by us using instanton theory<sup>14</sup>.

The asymmetry in molecules can also be found in some tautomers. In this case, potential energy surface does not possess a symmetry relating the wells and their shapes, and the minimum energies are different. A possible candidate belonging to this class is 2-hydroxy-1-naphthaldehyde, shown in Figure 1. Hydroxyl proton forms a hydrogen bond with the oxygen atom of the carbonyl group, and can tunnel to it to form a tautomer, which is a local minimum.

<sup>a)</sup> Author to whom correspondence should be addressed: mcvitas@irb.hr

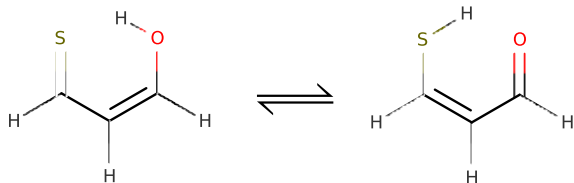


FIG. 2. Tunneling tautomers of thiomalonaldehyde.

Thiomalonaldehyde has two nearly degenerate minima in the form of enol and enethiol tautomers, shown in Figure 2. Enethiol is about  $70\text{ cm}^{-1}$  more stable<sup>15</sup>, with the barrier height to interconversion slightly lower than in the malonaldehyde. This implies that the TS is similar in magnitude to the energy asymmetry of the wells and the states in different wells that lie below the barrier are expected to interact. Interestingly, it has been suggested<sup>15</sup> that the replacement of hydrogen, shared by the hydrogen bonds OH-S and SH-O, by deuterium reverses the stability order of tautomers due to zero-point energy effect.

The asymmetry can also be caused by environment. Molecules in rare gas matrices can have energy asymmetry between the wells comparable to their TS in isolation. Delocalization of the tunneling hydrogen was observed<sup>16</sup> in 9-hydroxyphenalene embedded in a neon matrix. Molecules in crystals in the vicinity of a suitable guest molecule can also have comparable energies of the splittings and the energy asymmetry of the wells<sup>17</sup>.

Quantum tunneling has also been observed in macroscopic systems. tunneling of Bose-Einstein condensates<sup>18</sup>, electron spin tunneling in the nanomagnetic molecules<sup>19</sup> or the tunneling of magnetic flux in superconducting circuits based on Josephson junctions<sup>20</sup> are some recent examples. In a collective macroscopic variable, these processes can be described by a double well with externally controllable parameters that can induce asymmetry between the wells.

Calculation of TS in moderately large molecules is prohibitively costly. Exact variational methods for determining the bound states of molecules scale exponentially with the basis set size while large basis sets are often required<sup>21</sup>. Basis functions need to span over two or more wells sufficiently densely to obtain enough resolution to extract the splittings from the difference of the energies in their spectrum. The asymmetry of the wells also suggests that the symmetry cannot be used to reduce the size of the problem. Full-dimensional studies of malonaldehyde using multiconfigurational time-depended Hartree<sup>22,23</sup> (MCTDH), variational calculations on HF dimer<sup>21</sup> or H<sub>2</sub>O dimer<sup>24</sup> represent the state-of-the-art calculations of the vibrational levels using formally exact methods.

A direct calculation of TS in larger systems can be performed using a recently developed path integral molecu-

lar dynamics method<sup>25</sup> based on the potential sampling around the minimum action paths (MAP) connecting different wells. The multi-well splitting patterns of water trimer and hexamer<sup>26</sup> were obtained in this way using a matrix model of hamiltonian in the basis of local vibrational states. The tunneling matrix (TM) elements are extracted from the zero-temperature limit of the partition function, which means that the method only works for the vibrational ground-state in symmetric well systems.

Alternatively, the TM elements can be estimated using semiclassical methods. From that class, the instanton method, which comes in several forms<sup>27–30</sup>, has some particularly appealing features. It can be applied in Cartesian coordinates<sup>29,31</sup> to any molecule without modification. Numerically, it relies on the optimization of the minimum action path (MAP) that connects the symmetry-related minima<sup>32</sup>, and requires the potential and Hessians of the potential along the MAP to evaluate the splittings. It thus relies on a modest number of potential and gradient evaluations<sup>33</sup> in comparison with the exact quantum methods. This allows one to perform calculations in full dimensionality or in combination with on-the-fly evaluation of the electronic potential. Additionally, its accuracy is higher for large barriers and small splittings. Precisely in this regime, the exact variational methods become inefficient and resource intensive.

The first derivation of multidimensional instanton theory was accomplished by means of Jacobi fields integration (JFI)<sup>30</sup>. JFI method has been used to determine TS for a range of symmetric double-well systems, such as malonaldehyde<sup>30,32,33</sup>, vinyl radical<sup>34</sup>, and formic acid dimer<sup>35</sup>. The instanton method was later rederived in the ring polymer form (RPI)<sup>29</sup>, which could treat asymmetric potentials along MAPs and multiple wells. The RPI was used to calculate and interpret experimental ground-state splitting patterns of water clusters in terms of their rearrangement dynamics<sup>8</sup> for the dimer,<sup>29,36,37</sup> trimer<sup>29,38</sup> hexamer<sup>39</sup> and octamer<sup>40</sup>. We recently generalized the JFI method<sup>31</sup> to treat the multi-well systems and used it to explain the ground-state splitting pattern of 320 states in the water pentamer in terms of five dominant rearrangement pathways<sup>41</sup>. The extension of the method to low-lying vibrational states<sup>42</sup> is based on the work of Mil'nikov and Nakamura<sup>43</sup> and forms the groundwork of calculating the TM elements between local vibrational states of different wells in the present study below.

Weakly biased double-well systems have been considered in previous work by several authors. Analytical results in one dimension have been obtained using semiclassical WKB and instanton methods. Garg has demonstrated<sup>44</sup> that the instanton and the WKB method with Herring formula<sup>45</sup> give equivalent results for TS in symmetric systems. Cesi et al.<sup>46</sup> considered a one-dimensional (1D) double-well with the shape asymmetry and no energy asymmetry using instantons and obtained an expression for the ground-state TS. An approximate solution for a one-dimensional double well with a weak

bias was also obtained by Mugnai and Ranfagni<sup>47</sup>, using instantons based on the MAP that does not fully connect the minima of the two wells. Leggett *et al* obtained a solution<sup>48</sup> by adding a parabolic correction potential to remove the asymmetry between the wells, the contribution of which was then subsequently subtracted from the action integral. Dekker<sup>49</sup> derived the ground-state TS from the quantization condition by asymptotic matching of the semiclassical wavefunction in the barrier to the parabolic cylinder wavefunctions of harmonic oscillators in the two wells. Song<sup>50,51</sup> extended Dekker’s method<sup>49</sup> (as have Halataie and Leggett<sup>52</sup> done independently) to obtain the TS in vibrationally excited states of asymmetric 1D potentials with arbitrarily large shape and energy asymmetry. Song also showed<sup>51</sup> that the instanton wavefunctions with the Herring formula in a  $2 \times 2$  matrix model give equivalent results to those obtained by Dekker’s method<sup>49</sup>.

In multidimensional systems, tunneling can be assisted or suppressed by the excitation of the transversal vibrational modes<sup>43,53</sup>. In the presence of asymmetry, the excited states of one well can be in a resonance with the states of another well with a different set of local quantum numbers, which results in a delocalization of the wavefunction across these wells<sup>51</sup>. Benderskii *et al* devised a multidimensional perturbative instanton method<sup>54</sup> in which they treat the asymmetry of the potential in an analytic two-dimensional model as a correction of first order in  $\hbar$ , same as energy. In this way, the MAP remains symmetric and the asymmetry is moved to the transport equation along with energy. They also show that the equivalent expressions for the TS are obtained using the instanton quantization condition of Dekker<sup>49</sup> and using the instanton or WKB wavefunctions with Herring formula<sup>45</sup> in one dimension. The method was applied to calculate TSs in excited vibrational states of malonaldehyde<sup>55</sup> with the asymmetric isotopic substitutions, using a fit of model potential parameters to quantum-chemical data. The extensions of the RPI and JFI method to the ground-states of the asymmetric systems with a weak bias have recently been derived and applied to partially deuterated malonaldehyde<sup>9</sup> and water trimer<sup>14</sup>, respectively.

The object of this paper is to propose a method for calculating vibrational tunneling spectrum of multi-well systems of moderately sized molecules that are outside reach of the exact quantum methods. For this purpose, we extend the usual  $2 \times 2$  matrix model to the  $mN \times mN$  model, which represents the molecular Hamiltonian in the basis of  $N$  local vibrational states of  $m$  wells. We rederive a generalized Herring formula<sup>45,54</sup> in order to calculate the off-diagonal TM elements that represent the interaction of the local vibrational states of different wells. The semiclassical wavefunctions on the dividing plane, in the barrier that separates the wells, are obtained using the recently generalized JFI method<sup>31,43</sup>. The diagonal energies of the local vibrational states can be calculated using any accurate quantum method with a basis set that spans

only one well. Vibrational configuration interaction<sup>56–58</sup> (VCI) is used in this work. The effect of rotations is neglected.

The method, presented in Section II, allows one to study vibrational structure in asymmetric systems with multiple wells, separated by large potential barriers, in an approximate manner. The accuracy of the method is tested on a two-dimensional double-well model in Section III. In Section IV, it is applied to the (symmetric) malonaldehyde molecule, which tests the accuracy of the matrix model with the combination of VCI and JFI matrix elements in vibrationally excited states using a comparison with the exact MCTDH calculations. The vibrational tunneling spectrum of partially deuterated malonaldehyde is calculated in Section V, which features the mixing of inequivalent well states due to tunneling. The paper concludes in Section VI.

## II. TUNNELING MATRIX

Without the loss of generality, we start by considering a system with *two* minima separated by a large potential barrier. The minima, denoted as ‘left’ (L) and ‘right’ (R), are not necessarily symmetric either in shape or energy. For low-energy spectra, the vibrational Hamiltonian can be represented in the basis of states that are localized in the wells,  $\{\phi_i^{(L)}, \phi_j^{(R)}\}$ , as

$$\begin{pmatrix} \mathbf{H}^{(L)} & \mathbf{h} \\ \mathbf{h}^\top & \mathbf{H}^{(R)} \end{pmatrix}. \quad (1)$$

Square blocks  $\mathbf{H}^{(L/R)}$  are formed using basis functions of the same minimum and are not necessarily of equal size. Their off-diagonal elements describe the interaction between different basis functions localized in the same minimum and can be made small by a suitable choice of the basis. In the instanton theory of tunneling splittings, the usual presumption is that the local vibrational wavefunctions are harmonic oscillator states. In that case, the off-diagonal terms describe anharmonic contributions that originate from the difference between the full and the harmonic potential.

In our approach here, we replace the harmonic surface of each well by an  $n$ -mode representation<sup>59,60</sup> of the well potential and calculate local eigenfunctions and eigenvalues using vibrational self consistent field (VSCF) and vibrational configuration interaction (VCI) methods<sup>56–58</sup>. The technical details of the calculations are described in Appendix C. Using the more accurate local wavefunctions as a basis reduces the magnitude of the off-diagonal matrix elements in  $\mathbf{H}^{(L/R)}$ , which we then neglect. The matrices  $\mathbf{H}^{(L/R)}$  become diagonal and the diagonal matrix elements are referred to as the local vibrational energies of the left/right (L/R) well. For symmetric wells, the local energies are doubly degenerate.

The block  $\mathbf{h}$  in matrix (1) contains the TM elements that describe the interaction of local wavefunctions of the

left and right minimum. The exact quantal calculation of these elements requires a large basis set that can accurately represent the form of the wavefunction inside the barrier. Instead, we obtain them by means of the Herring formula<sup>45</sup> in combination with the semiclassical wavefunctions from the instanton theory<sup>42,43</sup>.

We now derive the Herring formula without the usual assumptions of the two-state model and the L/R symmetry. Rather, we consider the Schrödinger equation with the Hamiltonian matrix (1) from which it follows that

$$\begin{aligned}\hat{H}\phi_i^{(L)} &= E_i^{(L)}\phi_i^{(L)} + h_{ik}\phi_k^{(R)}, \\ \hat{H}\phi_j^{(R)} &= E_j^{(R)}\phi_j^{(R)} + h_{kj}\phi_k^{(L)},\end{aligned}\quad (2)$$

where  $E_i^{(L/R)}$  are local vibrational energies and the summation over repeated indices is assumed. Next, a dividing plane is defined inside the barrier via the implicit equation  $f(\mathbf{x}) = 0$ , which separates the left and right minimum. Eqns. (2) are multiplied by  $\phi_j^{(R)}$  and  $\phi_i^{(L)}$ , respectively, subtracted and integrated over the left part of the domain (i.e., over the space on the ‘left’ side of the dividing plane). The local wavefunctions  $\phi_i^{(L/R)}$ , either harmonic or VCI, have been obtained as eigenfunctions of a hermitian matrix and are therefore taken to be orthonormal. For a sufficiently high barrier, the wavefunctions  $\phi_i^{(L/R)}$  can be considered small in the R/L domain, respectively. We thus neglect the integrals involving the like products  $\phi_i^{(R)}\phi_i^{(R)}$  in the L volume and extend the integrals involving  $\phi_i^{(L)}\phi_j^{(L)}$  over the entire domain to produce  $\delta_{ij}$ . The integrals involving the mixed products  $\phi_i^{(L)}\phi_j^{(R)}$  have also been neglected. The error introduced with the neglect of these terms outside the resonance, i.e., for  $E_i^{(L)} \neq E_j^{(R)}$ , is analysed in more detail in Appendix B. The tunneling matrix element is then expressed as

$$\begin{aligned}h_{ij} &= \int_L \left( \phi_i^{(L)} \hat{H} \phi_j^{(R)} - \phi_j^{(R)} \hat{H} \phi_i^{(L)} \right) d\mathbf{x} \\ &= \frac{1}{2} \int_L \nabla \left( \phi_j^{(R)} \nabla \phi_i^{(L)} - \phi_i^{(L)} \nabla \phi_j^{(R)} \right) d\mathbf{x} \\ &= \frac{1}{2} \int \left( \phi_j^{(R)} \frac{\partial}{\partial S} \phi_i^{(L)} - \phi_i^{(L)} \frac{\partial}{\partial S} \phi_j^{(R)} \right) \delta(f(\mathbf{x})) d\mathbf{x},\end{aligned}\quad (3)$$

where, in the last step, we use the divergence theorem to turn the spatial integration into the integral over the dividing plane.  $S$  in Eq. (3) denotes the coordinate that describes an orthogonal shift from the dividing plane.

Local wavefunctions that we designed to calculate the local vibrational energies on the diagonal of matrix (1) are constructed using VSCF/VCI with a limited basis set and their accuracy drops inside the barrier that separates the wells. In order to evaluate the surface integral in Herring formula, Eq. (3), inside the barrier, we employ the instanton wavefunctions instead, which we recently derived in Ref. 42. These are based on the WKB method in which the energy is treated as a term of order  $\hbar^1$  and is moved

to the transport equation, leaving the Hamilton-Jacobi equation energy independent. It was shown that this approach gives equivalent results to the standard WKB method in 1D<sup>44</sup>. Moreover, the ground-state TS obtained from the Herring formula with the ground-state instanton wavefunctions<sup>42</sup> is identical to the standard instanton result derived from the steepest descent approximation of the partition function in the path integral formulation<sup>31</sup>.

The characteristic of the Hamilton-Jacobi equation that connects the minimum of a well to a point in configuration space obeys the equation<sup>42</sup>

$$\frac{d^2}{d\tau^2} \mathbf{x} = \nabla V, \quad (4)$$

and represents a classical trajectory  $\mathbf{x}(\tau)$  on the inverted PES, parametrized by the ‘imaginary’ time  $\tau$ . Local wavefunctions are expressed in terms of  $N$  local coordinates  $(S, \Delta\mathbf{x})$  defined in Refs. 42 and 43, where  $S$  is the mass-scaled arc length distance from the minimum along the characteristic and  $\Delta\mathbf{x}$  is the orthogonal shift from the nearest point on the characteristic. The classical momentum is defined as

$$p_0^{(L/R)} = \frac{dS}{d\tau} = \sqrt{2(V - V_{\min}^{(L/R)})}, \quad (5)$$

and  $S$  can be used to reparametrize the characteristic. Local wavefunctions in the harmonic vicinity of the characteristic are obtained by integrating the Hamilton-Jacobi and transport equations on the characteristic<sup>42</sup> as

$$\begin{aligned}\phi_\nu^{(L/R)} &= \sqrt[4]{\frac{\det \mathbf{A}_0^{(L/R)}}{\pi^N}} \sqrt{\frac{(2\omega_e^{(L/R)})^\nu}{(2\nu - 1)!!}} \\ &\times \left( F^{(L/R)} + \mathbf{U}^{(L/R)\top} \Delta\mathbf{x} \right)^\nu e^{-\int_0^S p_0^{(L/R)}(S') dS'} \\ &\times e^{-\frac{1}{2} \int_0^S \frac{\text{Tr}(\mathbf{A}^{(L/R)} - \mathbf{A}_0^{(L/R)})}{p_0^{(L/R)}(S')} dS' - \frac{1}{2} \Delta\mathbf{x}^\top \mathbf{A}^{(L/R)} \Delta\mathbf{x}}.\end{aligned}\quad (6)$$

For vibrationally excited states, the label  $\nu$  in Eq. (6) numbers the quanta in the excited vibrational mode of frequency  $\omega_e$ . Matrices  $\mathbf{A}^{(L/R)}$  are Gaussian widths of the wavefunction in the directions orthogonal to the characteristic and are obtained from

$$p_0^{(L/R)} \frac{d}{dS} \mathbf{A}^{(L/R)} = \mathbf{H}(S) - \left( \mathbf{A}^{(L/R)} \right)^2, \quad (7)$$

where  $\mathbf{H}$  is Hessian at  $S$  on the characteristic. The initial condition for Eq. (7) at the minimum is  $\mathbf{A}_0^{(L/R)} = \left( \mathbf{H}_0^{(L/R)} \right)^{1/2}$ , where  $\mathbf{H}_0^{(L/R)}$  is Hessian at the minimum (L/R). For vibrationally excited states, the prefactor in the parenthesis in Eq. (6) contains terms  $F(S)$  and  $\mathbf{U}(S)$ , which are defined via equations

$$\begin{aligned}p_0^{(L/R)} \frac{d}{dS} F^{(L/R)} &= \omega_e^{(L/R)} F^{(L/R)}, \\ p_0^{(L/R)} \frac{d}{dS} \mathbf{U}^{(L/R)} &= \omega_e^{(L/R)} \mathbf{U}^{(L/R)} - \mathbf{A}^{(L/R)} \mathbf{U}^{(L/R)}.\end{aligned}\quad (8)$$



$F^{(L/R)}$  terms account for the change in the amplitude of the excited-state wavefunction along the characteristic, while the  $\mathbf{U}^{(L/R)}$  term describes the nodal plane. Initial condition for  $F^{(L/R)}$  is found by matching the instanton wavefunction to that of the harmonic oscillator at a small distance  $S = \varepsilon$  from the minimum, as  $F^{(L/R)}(\varepsilon) = \mathbf{U}_0^{(L/R),\top}(\mathbf{x}(\varepsilon) - \mathbf{x}_{\min}^{(L/R)})$ , where  $\mathbf{U}_0^{(L/R)}$  is the initial condition  $\mathbf{U}^{(L/R)}(0)$  in Eq. (8) and the excited-state normal mode, i.e., the eigenvector of  $\mathbf{H}_0$  having frequency  $\omega_e$ .

The local instanton wavefunctions, Eq. (6), for the left and right minimum are next inserted into the Herring formula Eq. (3). For that purpose, a connection point  $\mathbf{x}(S_{\text{cp}})$  is chosen on the dividing surface  $f(\mathbf{x})$  inside the barrier and characteristics are determined which connect it to the minima on both sides of the dividing surface. The surface integral in Eq. (3) can then be computed analytically<sup>42</sup>.

This approach yields best results if the connection point is chosen so that both wavefunctions are near their maxima in the dividing plane at the connection point. This can be obtained by minimization of the sum of action integrals  $\int_0^{S_{\text{cp}}^{(L)}} p_0^{(L)}(S') dS' + \int_0^{S_{\text{cp}}^{(R)}} p_0^{(R)}(S') dS'$ . In the case of minima with the same energy, this procedure yields the minimum action path (MAP) that connects the minima and any point on that path is a suitable candidate for the connection point. The dividing surface can then be chosen as the plane orthogonal to the MAP at the connection point. If the minima do not have the same energies, but differ by the amount  $d$ , this procedure is equivalent to determining the MAP on the modified PES  $\tilde{V}(\mathbf{x}) = V(\mathbf{x}) - \Theta(S - S_{\text{cp}})d$ , where  $S_{\text{cp}}$  is the position of the connection point on the characteristic and  $\Theta$  is the Heaviside step function. In this case, the position of the connection point has to be given a priori, and the resulting path will depend on its position. The safest choice is to pick the connection point in the middle of the MAP, which is expected to be near the maximum of the potential energy barrier. Again, the dividing plane is taken to be orthogonal to the determined MAP and the surface integral is solved analytically. The TM element then becomes

$$h_{\nu\nu'} = -\sqrt{\frac{\sqrt{\det' \mathbf{A}_0^{(L)} \det' \mathbf{A}_0^{(R)}}}{\pi \det' \bar{\mathbf{A}}} \frac{p_0^{(L)} + p_0^{(R)}}{2}} \left[ \left( F^{(L)} \right)^\nu \left( F^{(R)} \right)^{\nu'} + \frac{1}{2} \mathbf{U}^{(L)} \bar{\mathbf{A}}^{-1} \mathbf{U}^{(R)} \delta_{1,\nu} \delta_{1,\nu'} \right] \sqrt{\frac{\left( 2\omega_e^{(L)} \right)^\nu \left( 2\omega_e^{(R)} \right)^{\nu'}}{(2\nu-1)!!(2\nu'-1)!!}} e^{-\int_0^{S_{\text{cp}}} p_0^{(L)} dS - \int_{S_{\text{cp}}}^{S_{\text{tot}}} p_0^{(R)} dS} e^{-\frac{1}{2} \int_0^{S_{\text{cp}}} \frac{\text{Tr}(\mathbf{A}^{(L)} - \mathbf{A}_0^{(L)})}{p_0^{(L)}} dS - \frac{1}{2} \int_{S_{\text{cp}}}^{S_{\text{tot}}} \frac{\text{Tr}(\mathbf{A}^{(R)} - \mathbf{A}_0^{(R)})}{p_0^{(R)}} dS}, \quad (9)$$

where  $S_{\text{tot}}$  is the total length of the MAP,  $\bar{\mathbf{A}} = \frac{\mathbf{A}^{(L)} + \mathbf{A}^{(R)}}{2}$  and  $\det'$  denotes a product of all non-zero

eigenvalues. Matrices  $\mathbf{A}_0$  have zero eigenvalues associated with the translations and rotations, while  $\bar{\mathbf{A}}$  has an additional zero eigenvalue that correspond to the tangent to the MAP. The TM element in Eq. (9) is valid for  $\nu, \nu' = 0, 1$ . For  $\nu > 1$ , the TM element can still be evaluated using Herring formula with analytical integrals but the form is more involved and we have only implemented it numerically without trying to write down the explicit form. We also remark here that the wavefunction in Eq. (6) for the multiply excited normal modes does not correspond to the harmonic oscillator wavefunction near the minimum, as the prefactor is not a Hermite polynomial. Thus, the matrix elements involving states with  $\nu > 1$  should not be taken as exact, but only as an estimate. The TM element, 9, is not invariant with respect to the position of the connection point  $S_{\text{cp}}$  unless the two local states are in resonance, as shown in Appendix B.

### III. NUMERICAL TESTS

Numerical tests were carried out on a model two-dimensional (2D) PES and on malonaldehyde molecule with some atoms substituted with heavier isotopes. MAPs were determined using the string method<sup>32,33</sup>. The criterion for convergence was chosen to be the largest component of gradient of Jacobi action perpendicular to the path and was set to  $10^{-6}$  a.u.. Number of beads used to discretize the string was 301 for model potential, which is much larger than necessary for convergence, but was used to ensure that all results obtained using different parameters of the potential are sufficiently converged. For potential with minima at different energies, the dividing plane was set to pass through the central bead of the MAP. In the case of malonaldehyde, the number of beads was 201 and the minima were oriented towards the first neighbouring bead in each step of the optimization to minimise the root-mean-square distance between their geometries<sup>32</sup>. After optimization, Hessians of the potential were determined at each bead on the MAP. Translations and rotations were explicitly projected out from Hessians<sup>31</sup>. Geometries along the path in mass-scaled Cartesian coordinates, potential and Hessian matrix elements were parametrized by the arc length along the MAP and interpolated using natural cubic splines. Matrices  $\mathbf{A}^{(L/R)}$  were propagated using the previously described approach<sup>42</sup>, with the initial ‘jump’ at  $\varepsilon = 0.1$  a.u. for model potential and  $\varepsilon = 0.25$  a.u. for malonaldehyde. Fourth order Runge-Kutta method was used to integrate Eq. (7). Matrices  $\mathbf{A}^{(L/R)}(S)$  were saved at each bead and their matrix elements interpolated using natural cubic splines, as for Hessians above. The interpolant was then used to propagate  $F^{(L/R)}$  and  $\mathbf{U}^{(L/R)}$  in Eq. (8). The dividing plane was set at the middle of the path.

The particular implementation of the VSCF/VCI method that is employed in our calculation here is described in Appendix C. We determined the 1-mode and 2-mode terms of the PES. In each normal mode, the po-

tential was evaluated at Gauss-Hermite discrete-variable-representation (DVR) points, which correspond to the zeroes of Hermite polynomials. For the 2D model potential 8 DVR points were used while for malonaldehyde we used 11 DVR points. This approach utilizes the natural lengthscales of the harmonic oscillators in each normal mode, which gives a balanced description of potential at different minima. 1-mode terms were then fitted to the eighth order polynomials using linear regression. For 2-mode terms, the potential was computed on the rectangular grid of DVR points determined above and a fit was performed analogously. For each 1-mode potential, a quick QM calculation was performed using sine DVR basis with 100 basis functions. The difference in the lowest two energies from that calculation was used as a frequency for the harmonic oscillator basis set, which was used to solve the VSCF equations. This approach provides a better basis for determining 1-mode potentials which quickly deviate from the harmonic curve, reducing the number of basis functions needed to describe 1-mode functions in VSCF.  $N_{\text{basis}} = 7$  and  $N_{\text{basis}} = 16$  basis functions were used for each normal mode for the 2D model potential and malonaldehyde, respectively, to converge the energies. A larger basis should not be used, as functions corresponding to larger energies begin to penetrate into unphysical part of the fitted potential, which can cause appearance of intruder states and worse energies. After VSCF calculation, the computed 1-mode functions were used for VCISD calculation, where the highest excitation in each mode was limited to 6 in both, the 2D model system and malonaldehyde.

### A. 2D MODEL POTENTIAL

The 2D model potential with two minima, which we use in our test calculations below, is defined by the following equations,

$$\begin{aligned}
 V(\mathbf{x}) &= \frac{\gamma_1 V^{(L)}(\gamma_2 V^{(R)} + d)}{\gamma_1 V^{(L)} + \gamma_2 V^{(R)}}, \\
 V^{(L)}(\mathbf{x}) &= \frac{1}{2} \Delta \mathbf{x}^{(L)\top} \mathbf{U}^{(L)} \begin{pmatrix} \alpha_{1,L} & 0 \\ 0 & \alpha_{2,L} \end{pmatrix} \mathbf{U}^{(L)\top} \Delta \mathbf{x}^{(L)}, \\
 V^{(R)}(\mathbf{x}) &= \frac{1}{2} \Delta \mathbf{x}^{(R)\top} \mathbf{U}^{(R)} \begin{pmatrix} \alpha_{1,R} & 0 \\ 0 & \alpha_{2,R} \end{pmatrix} \mathbf{U}^{(R)\top} \Delta \mathbf{x}^{(R)}, \\
 \mathbf{U}^{(L)} &= \begin{pmatrix} \cos \theta & -\sin \theta \\ \sin \theta & \cos \theta \end{pmatrix}, \quad \mathbf{U}^{(R)} = \begin{pmatrix} -\cos \theta & \sin \theta \\ \sin \theta & \cos \theta \end{pmatrix}, \\
 \Delta \mathbf{x}^{(L/R)} &= \mathbf{x} - \mathbf{x}^{(L)}, \quad \mathbf{x}^{(L/R)} = (\pm\beta, 0)^\top, \\
 \gamma_1 &= \frac{1 + \frac{d^2}{V^{(L)}(\mathbf{x}^{(R)})V^{(R)}(\mathbf{x}^{(L)})}}{1 + \frac{d}{V^{(R)}(\mathbf{x}^{(L)})}}, \quad \gamma_2 = \frac{1 + \frac{d^2}{V^{(L)}(\mathbf{x}^{(R)})V^{(R)}(\mathbf{x}^{(L)})}}{1 - \frac{d}{V^{(L)}(\mathbf{x}^{(R)})}},
 \end{aligned} \tag{10}$$

where  $\mathbf{x}$  are not mass scaled. Minima are located at  $\mathbf{x}^{(L/R)}$ . Coefficients  $\gamma_1$  and  $\gamma_2$  are chosen so that in the vicinity of left minimum, the potential is approximately harmonic and equals  $V \approx V^{(L)}$ , while in the

vicinity of the right minimum, the potential is approximately harmonic and shifted in energy by  $d$ , i.e.,  $V \approx V^{(R)} + d$ .  $\alpha_{1,L/R}$  and  $\alpha_{2,L/R}$  are eigenvalues of Hessian, while  $\mathbf{U}^{(L/R)}$  are normal modes. Parameter  $\theta$  denotes the angle between normal modes in the left and right minimum. Mass of the system was taken to be  $m = 3.5$  in both dimensions, so that the harmonic frequencies are given by  $\omega_{1/2}^{(L/R)} = \sqrt{\alpha_{1/2,L/R}/m}$ .

The above form of the potential can be used to independently vary harmonic frequencies  $\omega_{1/2}^{(R)}$ , by changing parameters  $\alpha_{1/2,R}$ , or the shift  $d$  without affecting the other parameters of either the left or the right minimum. In this paper, the parameters of the left minimum were  $\alpha_{1,L} = 1.6$ ,  $\alpha_{2,L} = 4.0$ , while the parameters of the right minimum were the same as the parameters of the left, for the symmetric case with  $d = 0$ . To obtain asymmetric potentials below, one of the three parameters was varied, with  $\alpha_{1,R}$  going from 1.6 to 36.0, parameter  $\alpha_{2,R}$  going from 4.0 to 49.0 and  $d$  going from 0.0 to 1.1. Positions of the minima were set with  $\beta = 2.0$  and the angle between the normal modes was chosen as  $\theta = \pi/12$ . This angle corresponds to approximately equal contributions of  $F^{(L/R)}$  and  $\mathbf{U}^{(L/R)}$  in the TM elements<sup>42</sup>. Figure 4 shows the model potential for a selection of parameters  $\alpha_{1,R}$ ,  $\alpha_{2,R}$  and  $d$ .

Frequency  $\omega_1$  is the lower frequency and the MAP enters the minima along the corresponding normal mode. Consequently,  $\omega_1$  does not contribute towards the zero-point energy in the plane orthogonal to the MAP. The effective barrier for the tunneling motion from the ground state in the left minimum, corrected by the zero-point motion contribution, can be defined as

$$V_{\text{eff}}^{(L)} = V_{\text{max}} + \frac{1}{2}(\lambda^{(L)} - \omega_1^{(L)} - \omega_2^{(L)}). \tag{11}$$

$V_{\text{max}}$  in Eq. (11) is the maximum of the potential  $V(S_{\text{max}})$  along the MAP.  $\lambda^{(L)}$  is the non-zero eigenvalue of  $\mathbf{A}_\perp = \mathbf{P}\mathbf{A}\mathbf{P}$  matrix, where  $\mathbf{P}$  projects out the tangent direction to the MAP, with all quantities evaluated at the position of the maximum,  $S = S_{\text{max}}$ . Analogously, the effective barrier can be defined for other states. Figure 5 (in the second column panels) shows that for the symmetric case,  $\omega_1^{(R)} = \omega_1^{(L)}$ , the instanton theory provides accurate tunneling splittings in the ground state and in the second excited state, which corresponds to the excitation of the transversal frequency  $\omega_2$ . In the first excited state, instanton theory slightly overestimates the TS. In that state, the effective barrier is much smaller and equals  $V_{\text{eff}} = 0.545$ , in contrast with the barriers of 1.221 and 0.976 for the ground and second excited state. This overestimation is a known property of the instanton method and has been noted previously<sup>42</sup>. In the symmetric case, the only contribution to the splitting comes from the off-diagonal matrix elements, so that the harmonic and VCI energies yield same results. However, it can be observed (from the first column panels in Figure 5) that the harmonic vibrational energies overestimate

the exact quantum-mechanical (QM) energies by 3 – 5%.

As the frequency  $\omega_1^{(R)}$  is increased and the difference in the local L/R energies begins to contribute to the overall splitting, the TS's computed using harmonic energies quickly begin to deviate from the QM values due to the neglect of anharmonicities, which no longer cancel out. When the difference in the lower frequency,  $\omega_1^{(R)} - \omega_1^{(L)}$  is only 0.02, which corresponds to the asymmetry ( $\Delta\omega_1/\omega_1^{(L)}$ ) of 3%, the error in the TS of the ground state is 24%, while it is 90% for the transversal mode ( $\omega_2$ ) excitation. A larger error in the excited state reflects the fact that the local excited-state wavefunction penetrates deeper into the barrier, where anharmonicity is larger. However, it can be seen that the VCI energies correctly account for the anharmonicities and provide an excellent agreement, as can be observed in the first column panels in Figure 5, both in the absolute energies and in the tunneling splittings (second column panels in Figure 5).

With a further increase in the frequency  $\omega_1^{(R)}$ , different local vibrational states of the left and right minimum enter into resonance and vibrational energies exhibit avoided crossings, shown in frames IV–VI of the top panel in Figure 5. Harmonic energies do not provide accurate positions of these avoided crossings, as seen in Figure 5, due to errors in the local energies. In the case of the avoided crossing between the higher-frequency  $\omega_2^{(L)}$ -excited state of the left minimum and the  $\omega_1^{(R)}$ -excited state of the right minimum, shown in frame IV of the top panel in Figure 5, the error in the position of the avoided crossing (in  $\omega_1^{(R)} - \omega_1^{(L)}$ ) using harmonic energies is 16% (and falls outside the frame IV in Figure 5). VCI energies, shown magnified in Figure 6 together with the exact QM energies, provide a significantly more accurate position with the error of only 0.4%. The small discrepancy can be attributed to the fact that, as frequency  $\omega_1^{(R)}$  is increased, the local wavefunction in the right minimum penetrates deeper into the barrier. In this region, the approximate  $n$ -mode representation of the potential used in the VCI calculations begins to deviate from the real potential, which introduces an error in the local energies.

The TS in the avoided crossing is reproduced with great accuracy, shown as the minima in the lower panel in Figure 6, with the error of 5%. Errors in the positions of other avoided crossings (IV–VI in Figure 5), namely between the ground state of the right minimum and the  $\omega_1^{(L)}$ - and  $\omega_2^{(L)}$ -excited states in the left minimum (frames V and VI in Figure 5, respectively) become larger even using VCI energies. This is again a consequence of larger asymmetries. The local wavefunction of the right minimum has larger energies and penetrates deeper into the region where the  $n$ -mode representation of the potential becomes unreliable. Nevertheless, the tunneling splittings in the avoided crossings are reproduced with great accuracy, which indicates that the instanton method can indeed give reliable TM elements between different vibra-

tional states of L/R minima and, in combination with the VCI energies, is a useful tool for computing vibrational tunneling spectra. Similar results were observed with the frequency  $\omega_2^{(R)}$  varied.

Figure 7 shows the dependence of energy levels with the variation in the depth of the right minimum  $d$ . Overall, the introduction of the energy asymmetry between the wells results in a similar behaviour to that observed above. A notable difference is that, in this case, the splittings obtained using harmonic energies are much closer to the exact QM values. This is an artefact of the construction of the PES, in which the frequencies in the left and right minimum are the same. As a result, the shapes of the local potentials in both minima are similar and a large part of the error introduced by the anharmonicity cancels out. However, in realistic applications, it is unlikely that systems with minima of different energies have same L/R frequencies. The error in the position of the avoided crossing IV is also much smaller for harmonic energies ( $\approx 2\%$ ), while it is again smaller using VCI energies (0.7%), as shown in Figure 8. The error in the TS in the avoided crossing is 12%, which is comparable to the error in the case of different frequencies, shown in Figure 6.

## B. MALONALDEHYDE

We next employ our combined approach to study the symmetric, homoisotopic malonaldehyde on the PES developed by Wang *et al*<sup>61</sup>. The molecule is shown labelled in the top panel in Figure 3. It has two equivalent wells with hydrogen 6 attached to either oxygen 1 or 5. We study below the effect of adding additional states in the tunneling matrix. For this purpose, vibrational energies are computed either from a  $2 \times 2$  matrix involving corresponding states in the two wells, a  $8 \times 8$  matrix involving 4 local states at both sides of the barrier and a  $16 \times 16$  matrix model. Thereby, we again calculate the local single-well states using VSCF/VCI, while the TM matrix elements are computed using our recently developed instanton method<sup>42</sup>.

Malonaldehyde has been extensively studied in the past<sup>62</sup> and presents a benchmark system for the development of quantum dynamical methods. Most recent calculations on the same PES using exact quantum methods were obtained using multiconfigurational time-dependent Hartree (MCTDH) by Hammer and Manthe<sup>23</sup> and Schröder and Meyer<sup>22</sup> and show a good level of agreement with experimental results<sup>63</sup>. We use the results of Ref. 23 for comparison, as they report tunneling splittings for a number of vibrationally excited states having a large transition dipole moment and are believed to be more accurate<sup>22</sup>.

Local harmonic and VSCF/VCI energies calculated in a 2-mode representation of a single well, as described in Appendix C, for the lowest 8 vibrational states, that we consider below, are shown in Table I. The ground state is

labelled GS, while the excited states are labelled by the frequencies of the excited normal modes  $\nu_i$ , numbered in the order of increasing frequency in the subscript, and separated by a '+' sign for multiple excitations. A noticeable shift can be observed between all harmonic and VCI energies in Table I due to anharmonicity, but the order in energy remains unchanged. The lowest four normal modes that can be excited in the lowest 8 local vibrational states and play a role in our calculations below are depicted in Figure 3. Higher single-well vibrational states become densely-spaced in energy and start to mix the excited vibrational modes at minima. Our approach relies on being able to uniquely define the excited normal modes at minima for each local vibrational state considered, because the instanton wavefunctions, that are used to calculate the tunneling matrix elements that connect these states, tend to harmonic oscillator eigenstates at minima. Moreover, a higher density of states at higher energies would require inclusion of many additional states in the tunneling matrix, which are not known as precisely as for the low-lying states and would degrade the accuracy. We limit ourselves, therefore, to the lowest 8 local states in the studies on tunneling spectra of malonaldehyde below.

State	Harmonic	VCI
GS	14950.11 (0.00)	14682.46 (0.00)
$\nu_1$	15218.68 (268.57)	15012.65 (330.19)
$\nu_2$	15245.53 (295.42)	15042.51 (360.05)
$\nu_3$	15333.29 (383.17)	15133.95 (451.49)
$\nu_1 + \nu_1$	15487.25 (537.14)	15262.05 (579.59)
$\nu_4$	15472.20 (522.08)	15281.89 (599.43)
$\nu_2 + \nu_2$	15540.95 (590.83)	15318.85 (636.40)
$\nu_1 + \nu_2$	15514.10 (563.99)	15336.16 (653.70)

TABLE I. Harmonic and VCI energies in  $\text{cm}^{-1}$  of the first 8 local vibrational states of malonaldehyde. The values relative to the lowest vibrational level are given in parentheses.

The TM elements of the  $\mathbf{h}$  matrix that connect the two sets of local states in the L and R wells are calculated using instanton theory and listed in Table II. Both minima of malonaldehyde belong to the  $C_s$  symmetry group and its local vibrational states can be classified according to the irreducible representation of the excited normal mode  $\nu_i$  at the minimum. The  $C_s$  symmetry is preserved along the MAP, so that the TM elements that connect normal modes of different symmetry vanish exactly, as seen in Table II.

In a  $2 \times 2$  matrix model, only the diagonal elements of  $\mathbf{h}$  matrix are used and the degenerate vibrational states of

L/R wells are split into doublets. The equivalent results are obtained using the first-order perturbation theory for degenerate states, yielding the tunneling splitting of  $\Delta_i = 2h_{ii}$ . Energies of the GS and the first 3 excited states obtained in this manner already show a good agreement with the MCTDH values of Ref. 23, as can be seen in Table III (from the second and the last column). The vibrational states are numbered in order of increasing energy in Table III. The wavefunction content, obtained from the eigenvectors of the TM, is listed in Table IV and can be used to identify state in Table III in terms of the excited normal modes.

The TS's for the GS and the singly excited modes  $\nu_{1-4}$  in the  $2 \times 2$  TM model are obtained as  $\Delta(\text{GS}) = 24.60\text{cm}^{-1}$ ,  $\Delta(\nu_1) = 13.40\text{cm}^{-1}$ ,  $\Delta(\nu_2) = 88.40\text{cm}^{-1}$ ,  $\Delta(\nu_3) = 17.06\text{cm}^{-1}$ ,  $\Delta(\nu_4) = 15.64\text{cm}^{-1}$ . The MCTDH results<sup>23</sup> for the TS's in the same states are  $\Delta(\text{GS}) = 23.5\text{cm}^{-1}$ ,  $\Delta(\nu_1) = 6.7\text{cm}^{-1}$ ,  $\Delta(\nu_2) = 69.9\text{cm}^{-1}$ ,  $\Delta(\nu_3) = 16.3\text{cm}^{-1}$ ,  $\Delta(\nu_4) = 18.8\text{cm}^{-1}$ . Differences of all TS's apart from the  $\nu_1$  and  $\nu_2$  excited modes are well within the estimated error of the MCTDH calculations, which validates the accuracy of our approach. The  $\nu_2$  mode corresponds to the longitudinal mode as it lies parallel to the MAP at minima. The excitation of this mode effectively lowers the barrier of the tunneling motion and the instanton theory is known to overestimate results in the shallow tunneling regime<sup>29,42</sup>. The wavefunction also penetrates deeper into the barrier where the anharmonic effects are larger and the VCI energies degrade as a result. Thus the absolute energies in Table III are expected to be affected for these states as well. The large increase in the TS for the excitation of the longitudinal mode is however expected and confirmed by the instanton theory<sup>42</sup>. The TS for the  $\nu_1$  mode is overestimated by a factor of two. This is most likely due to the anharmonicity along this normal mode, indicated by the large difference between the harmonic (268.57  $\text{cm}^{-1}$ ) and VCI (330.19  $\text{cm}^{-1}$ ) energies. Since the TS for the pair of states is significantly suppressed compared to the GS, the frequency and energy in its direction change significantly along the MAP. Therefore, if the anharmonicity also changes significantly, it could cause of the observed discrepancy. As an aside, we also note here that the other TS's computed using MCTDH in Ref. 23, which do not result in the mixture of normal modes at minima, are  $\Delta(\nu_5) = 21.1 \text{ cm}^{-1}$ ,  $\Delta(\nu_7) = 33.3 \text{ cm}^{-1}$ ,  $\Delta(\nu_8) = 14.6 \text{ cm}^{-1}$  and  $\Delta(\nu_{11}) = 19.5 \text{ cm}^{-1}$ , and are in good agreement with the values we obtain using instanton theory as  $\Delta(\nu_5) = 24.4 \text{ cm}^{-1}$ ,  $\Delta(\nu_7) = 39.5 \text{ cm}^{-1}$ ,  $\Delta(\nu_8) = 15.6 \text{ cm}^{-1}$  and  $\Delta(\nu_{11}) = 22.1 \text{ cm}^{-1}$ .

We next consider constructing the tunneling matrix of 4 local states of each well. This takes into account interactions between doublets considered above, whereby only the states of the same symmetry interact, as already discussed. If the states of the same symmetry are well separated with respect to the size of their TM element, the shift in energy can also be computed using the second-order perturbation theory. When 4 local states are taken



	$GS^{(R)}$	$\nu_1^{(R)}$	$\nu_2^{(R)}$	$\nu_3^{(R)}$	$(\nu_1 + \nu_1)^{(R)}$	$\nu_4^{(R)}$	$(\nu_2 + \nu_2)^{(R)}$	$(\nu_1 + \nu_2)^{(R)}$
$GS^{(L)}$	-12.30	0.00	-21.94	0.00	-4.98	-4.62	-25.53	0.00
$\nu_1^{(L)}$	0.00	-6.70	0.00	6.85	0.00	0.00	0.00	-11.95
$\nu_2^{(L)}$	-21.94	0.00	-44.20	0.00	-8.87	-7.54	-55.97	0.00
$\nu_3^{(L)}$	0.00	6.86	0.00	8.53	0.00	0.00	0.00	12.22
$(\nu_1 + \nu_1)^{(L)}$	-4.98	0.00	-8.88	0.00	-4.84	-1.87	-9.14	0.00
$\nu_4^{(L)}$	-4.61	0.00	-7.53	0.00	-1.87	7.82	-8.14	0.00
$(\nu_2 + \nu_2)^{(L)}$	-25.53	0.00	-55.97	0.00	-9.14	-8.15	-75.86	0.00
$(\nu_1 + \nu_2)^{(L)}$	0.00	-11.95	0.00	12.22	0.00	0.00	0.00	-21.31

TABLE II. Tunneling matrix elements for the first 8 local vibrational states of malonaldehyde.

No.	$E^{(pairs)}$	$E^{(4)}$	$E^{(8)}$	$E^{(MCTDH)}$
1	14670.15	14668.69	14667.08	14671.3
2	14694.76	14693.54	14692.76	14694.8
3	14998.31	14999.77	14987.74	14941.5
4	15005.95	15005.60	15005.09	15008.2
5	15019.35	15018.91	15018.54	15014.9
6	15086.70	15087.92	15077.14	15005.4
7	15125.42	15125.86	15125.14	15108.3
8	15142.47	15142.82	15142.04	15124.6
9	15243.00	-	15249.04	-
10	15257.21	-	15263.41	-
11	15266.89	-	15266.12	-
12	15274.07	-	15273.84	15249.6
13	15289.71	-	15291.11	15268.4
14	15314.85	-	15316.14	-
15	15357.47	-	15358.55	-
16	15394.71	-	15407.27	-

TABLE III. Vibrational energy levels of malonaldehyde obtained from local VCI energies either by splitting pairs of degenerate levels, or by diagonalizing model tunneling matrix constructed from 4 or 8 local states in each minimum. For reference, MCTDH energies are given where available.

into account in the  $8 \times 8$  TM model, slight shifts are observed in the GS and  $\nu_2$  doublets in Figure 9 (left-side spectrum). The absolute energies change by  $1.22 - 1.46 \text{ cm}^{-1}$ , while perturbation theory gives the shift of  $1.34 \text{ cm}^{-1}$ . However, the change in the TS is negligible.

In the  $16 \times 16$  TM model, consisting of 8 local states in both wells, a strong interaction with the doubly-excited  $(\nu_2 + \nu_2)$  mode causes a significant shift in the energies of the GS and  $\nu_2$ -excited doublets as well as their splittings. The TS's change from  $24.85 \text{ cm}^{-1}$  to  $25.68 \text{ cm}^{-1}$  and from  $88.15 \text{ cm}^{-1}$  to  $89.4 \text{ cm}^{-1}$ , which can clearly be observed in Figure 9 (right-side spectrum). A particularly strong mixing also occurs between the doubly-excited  $(\nu_2 + \nu_2)$  mode and the doubly-excited  $(\nu_1 + \nu_1)$  mode, for which the lower levels in the respective doublets are very close in energy ( $14.21 \text{ cm}^{-1}$ ) and they interact strongly ( $\hbar = 9.14 \text{ cm}^{-1}$  in Table II). The mixing results in visible changes in the dominant coefficients of TM eigenvectors in Table IV and results in observable energy shifts. Furthermore, singly-excited  $\nu_4$  mode interacts and mixes with the doubly-excited  $(\nu_1 + \nu_1)$  mode, which re-

sults in the change of TS from  $15.64 \text{ cm}^{-1}$  to  $17.27 \text{ cm}^{-1}$ , which is in closer agreement with the MCTDH value of  $18.8 \text{ cm}^{-1}$ . Finally, we remark that the TS of the doubly-excited  $(\nu_1 + \nu_2)$  state amounts to  $42.62 \text{ cm}^{-1}$  which is in good agreement with  $49.5 \text{ cm}^{-1}$  obtained by Schröder and Meyer<sup>22</sup>.

The above results clearly show that the interactions of different vibrational states can have a non-negligible effect, both, on the absolute values of the vibrational energies and on the values of the tunneling splittings. This effect is especially pronounced if two or more states of the same symmetry are close in energy and if the TM elements that connect them are large. This scenario is expected to play a significant role in the higher vibrationally excited states, where the density of states becomes larger and the interactions increase due to the presence of multiple excitations.

### C. PARTIALLY DEUTERATED MALONALDEHYDE

In the previous Subsection, we have learned what accuracy one might expect in the calculation of the tunneling spectra of malonaldehyde through comparison with the exact QM results. We now consider the partially deuterated (PD) malonaldehyde, where hydrogen in the position 7/9 is substituted by deuterium (see Figure 3) and the system is no longer symmetric. Since deuterium is not placed in equivalent positions in the two minima, their local vibrational frequencies and energies are no longer equal, even though the PES and barrier shapes remain unchanged. The particular choice of deuteration was chosen for our study because the mixing angle in its GS was determined experimentally by Baughcum *et al*<sup>10</sup> and the TS by Jahr *et al*<sup>9</sup> using RPI method. Furthermore, the size of the relative energy shifts between the left and right minimum is comparable to the size of the TM elements, which makes the system interesting in that both the VCI energies and the instanton TM elements are expected to make a significant contribution to the TS's in this system.

In the PD malonaldehyde, the isotopic substitution causes a significant lowering of the zero-point energy, given in Table V, from  $14682.45 \text{ cm}^{-1}$  to  $13978.19 \text{ cm}^{-1}$

No.	Pairs	(8)
1	0.707  GS <sup>(L)</sup> ⟩ 0.707  GS <sup>(R)</sup> ⟩	0.704  GS <sup>(L)</sup> ⟩ 0.704  GS <sup>(R)</sup> ⟩
2	0.707  GS <sup>(L)</sup> ⟩ -0.707  GS <sup>(R)</sup> ⟩	0.704  GS <sup>(L)</sup> ⟩ -0.704  GS <sup>(R)</sup> ⟩
3	0.707  ν <sub>2</sub> <sup>(L)</sup> ⟩ 0.707  ν <sub>2</sub> <sup>(R)</sup> ⟩	0.688  ν <sub>2</sub> <sup>(L)</sup> ⟩ 0.688  ν <sub>2</sub> <sup>(R)</sup> ⟩
4	0.707  ν <sub>1</sub> <sup>(L)</sup> ⟩ 0.707  ν <sub>1</sub> <sup>(R)</sup> ⟩	0.706  ν <sub>1</sub> <sup>(L)</sup> ⟩ 0.706  ν <sub>1</sub> <sup>(R)</sup> ⟩
5	0.707  ν <sub>1</sub> <sup>(L)</sup> ⟩ -0.707  ν <sub>1</sub> <sup>(R)</sup> ⟩	0.705  ν <sub>1</sub> <sup>(L)</sup> ⟩ -0.705  ν <sub>1</sub> <sup>(R)</sup> ⟩
6	0.707  ν <sub>2</sub> <sup>(L)</sup> ⟩ -0.707  ν <sub>2</sub> <sup>(R)</sup> ⟩	0.695  ν <sub>2</sub> <sup>(L)</sup> ⟩ -0.695  ν <sub>2</sub> <sup>(R)</sup> ⟩
7	0.707  ν <sub>3</sub> <sup>(L)</sup> ⟩ -0.707  ν <sub>3</sub> <sup>(R)</sup> ⟩	0.705  ν <sub>3</sub> <sup>(L)</sup> ⟩ -0.705  ν <sub>3</sub> <sup>(R)</sup> ⟩
8	0.707  ν <sub>3</sub> <sup>(L)</sup> ⟩ 0.707  ν <sub>3</sub> <sup>(R)</sup> ⟩	0.704  ν <sub>3</sub> <sup>(L)</sup> ⟩ 0.704  ν <sub>3</sub> <sup>(R)</sup> ⟩
9	0.707  ν <sub>2</sub> + ν <sub>2</sub> <sup>(L)</sup> ⟩ 0.707  ν <sub>2</sub> + ν <sub>2</sub> <sup>(R)</sup> ⟩	0.447  ν <sub>1</sub> + ν <sub>1</sub> <sup>(L)</sup> ⟩ 0.522  ν <sub>2</sub> + ν <sub>2</sub> <sup>(L)</sup> ⟩ 0.447  ν <sub>1</sub> + ν <sub>1</sub> <sup>(R)</sup> ⟩ 0.522  ν <sub>2</sub> + ν <sub>2</sub> <sup>(R)</sup> ⟩
10	0.707  ν <sub>1</sub> + ν <sub>1</sub> <sup>(L)</sup> ⟩ 0.707  ν <sub>1</sub> + ν <sub>1</sub> <sup>(R)</sup> ⟩	0.547  ν <sub>1</sub> + ν <sub>1</sub> <sup>(L)</sup> ⟩ -0.436  ν <sub>2</sub> + ν <sub>2</sub> <sup>(L)</sup> ⟩ 0.547  ν <sub>1</sub> + ν <sub>1</sub> <sup>(R)</sup> ⟩ -0.436  ν <sub>2</sub> + ν <sub>2</sub> <sup>(R)</sup> ⟩
11	0.707  ν <sub>1</sub> + ν <sub>1</sub> <sup>(L)</sup> ⟩ -0.707  ν <sub>1</sub> + ν <sub>1</sub> <sup>(R)</sup> ⟩	0.693  ν <sub>1</sub> + ν <sub>1</sub> <sup>(L)</sup> ⟩ -0.693  ν <sub>1</sub> + ν <sub>1</sub> <sup>(R)</sup> ⟩
12	0.707  ν <sub>4</sub> <sup>(L)</sup> ⟩ -0.707  ν <sub>4</sub> <sup>(R)</sup> ⟩	0.693  ν <sub>4</sub> <sup>(L)</sup> ⟩ -0.693  ν <sub>4</sub> <sup>(R)</sup> ⟩
13	0.707  ν <sub>4</sub> <sup>(L)</sup> ⟩ 0.707  ν <sub>4</sub> <sup>(R)</sup> ⟩	0.693  ν <sub>4</sub> <sup>(L)</sup> ⟩ 0.693  ν <sub>4</sub> <sup>(R)</sup> ⟩
14	0.707  ν <sub>1</sub> + ν <sub>2</sub> <sup>(L)</sup> ⟩ 0.707  ν <sub>1</sub> + ν <sub>2</sub> <sup>(R)</sup> ⟩	0.705  ν <sub>1</sub> + ν <sub>2</sub> <sup>(L)</sup> ⟩ 0.705  ν <sub>1</sub> + ν <sub>2</sub> <sup>(R)</sup> ⟩
15	0.707  ν <sub>1</sub> + ν <sub>2</sub> <sup>(L)</sup> ⟩ -0.707  ν <sub>1</sub> + ν <sub>2</sub> <sup>(R)</sup> ⟩	0.706  ν <sub>1</sub> + ν <sub>2</sub> <sup>(L)</sup> ⟩ -0.706  ν <sub>1</sub> + ν <sub>2</sub> <sup>(R)</sup> ⟩
16	0.707  ν <sub>2</sub> + ν <sub>2</sub> <sup>(L)</sup> ⟩ -0.707  ν <sub>2</sub> + ν <sub>2</sub> <sup>(R)</sup> ⟩	0.691  ν <sub>2</sub> + ν <sub>2</sub> <sup>(L)</sup> ⟩ -0.691  ν <sub>2</sub> + ν <sub>2</sub> <sup>(R)</sup> ⟩

TABLE IV. Dominant configurations of vibrational states of malonaldehyde, computed either by splitting pairs of degenerate states or by diagonalizing model Hamiltonian constructed with 8 localized states in each minimum.

for D7 minimum and 14013.04 cm<sup>-1</sup> for D9 minimum. Additionally, the excitation energies for the first 7 excited states decrease as well, by up to 40 cm<sup>-1</sup>. As a result, the vibrational states are more closely spaced, see Figure 10, and larger interstate L/R mixings are expected.

The normal modes in PD malonaldehyde are qualitatively similar to the homoisotopic malonaldehyde. The ordering of local single-well states, labelled by the excited normal mode at minimum, is also preserved upon deuteration, with the exception of the |ν<sub>1</sub> + ν<sub>2</sub><sup>(D9)</sup>⟩ and |ν<sub>2</sub> + ν<sub>2</sub><sup>(D9)</sup>⟩ states, which change order. The TM elements shown in Table VI, are remarkably similar to the homoisotopic malonaldehyde, which indicates that the wavefunctions in the barrier region are not significantly affected by the asymmetry. The error estimates due to the variation in the position of the dividing plane in Table VI are discussed in more detail in Appendix B.

State	Harmonic		VCI	
	D7	D9	D7	D9
GS	14228.18 (0.00)	14253.67 (25.49)	13978.19 (0.00)	14013.04 (34.85)
ν <sub>1</sub>	14492.55 (264.37)	14492.10 (263.92)	14298.70 (320.51)	14311.75 (333.56)
ν <sub>2</sub>	14522.65 (294.47)	14547.57 (319.39)	14327.02 (348.83)	14361.38 (383.19)
ν <sub>3</sub>	14568.85 (340.67)	14626.56 (398.38)	14384.49 (406.30)	14444.96 (466.76)
ν <sub>1</sub> + ν <sub>1</sub>	14756.92 (528.74)	14546.67 (502.34)	14950.11 (568.48)	14543.15 (564.96)
ν <sub>4</sub>	14744.31 (516.13)	14769.16 (540.98)	14562.35 (584.16)	14595.52 (617.32)
ν <sub>2</sub> + ν <sub>2</sub>	14817.13 (588.95)	14841.47 (613.29)	14601.27 (623.08)	14637.01 (658.82)
ν <sub>1</sub> + ν <sub>2</sub>	14787.02 (558.84)	14786.00 (557.82)	14614.31 (636.12)	14624.21 (646.02)

TABLE V. Harmonic and VCI energies in cm<sup>-1</sup> of the first 8 local vibrational states of partially deuterated malonaldehyde. The values relative to the lowest vibrational level of the D7 minimum are given in parentheses.

We again consider pairwise interactions of the corresponding states in a 2 × 2 TM model. This is possible since the normal modes at both minima can approximately be mapped to one another using a symmetry operation. The pairs of states are no longer degenerate in this case, and the first-order perturbation theory cannot be used to estimate the TS's. Instead, the TS, obtained from the eigenvalues of the TM, is seen to be equal to the local energy difference corrected by the second-order perturbative terms,

$$\Delta_i = \sqrt{(E_i^{(D7)} - E_i^{(D9)})^2 + 4h_{ii}^2} \\ \approx |E_i^{(D7)} - E_i^{(D9)}| + \frac{2h_{ii}^2}{|E_i^{(D7)} - E_i^{(D9)}|}, \quad (12)$$

where, in the last line of Eq. (12), we assumed that the TM element  $|h_{ii}| \ll |E_i^{(D7)} - E_i^{(D9)}|$ . This assumption is certainly violated if there are other local states which are energetically close and coupled by the TM elements that are comparable in size, as we shall see below.

The TM element for the GS is 12.32 cm<sup>-1</sup> using JFI method, which is in excellent agreement with 12.4 cm<sup>-1</sup> obtained by Jahr *et al*<sup>9</sup> using RPI. The mixing angle for the GS was estimated experimentally by Baughcum *et al*<sup>10</sup> at  $\phi = 41^\circ$ . The mixing angle was evaluated using local harmonic energies in Ref. 9 to  $\phi = 44^\circ$ . Using VCI energies, we estimate the mixing angle to be  $\phi = 35.3^\circ$ , which indicates that the anharmonicity is indeed responsible for a decrease in its value, as speculated by Jahr *et al*<sup>9</sup>. We are also able to estimate the effect of inclusion of other local vibrational states on the mixing angle from the components of the eigenvectors of the TM as

$$\tan \phi/2 = \frac{c(\text{GS}^{(D9)})}{c(\text{GS}^{(D7)})} \quad (13)$$

	$\text{GS}^{(\text{D9})}$	$\nu_1^{(\text{D9})}$	$\nu_2^{(\text{D9})}$	$\nu_3^{(\text{D9})}$	$(\nu_1 + \nu_1)^{(\text{D9})}$	$\nu_4^{(\text{D9})}$	$(\nu_2 + \nu_2)^{(\text{D9})}$	$(\nu_1 + \nu_2)^{(\text{D9})}$
$\text{GS}^{(\text{D7})}$	-12.32 (0.005)	0.00 (0.00)	-21.95 (0.133)	0.00 (0.00)	-5.04 (0.042)	-4.63 (0.034)	-25.54 (0.343)	0.00 (0.00)
$\nu_1^{(\text{D7})}$	0.00 (0.00)	-6.86 (0.001)	0.00 (0.00)	6.52 (0.014)	0.00 (0.00)	0.00 (0.00)	0.00 (0.00)	-12.22 (0.077)
$\nu_2^{(\text{D7})}$	-21.89 (0.109)	0.00 (0.00)	-44.12 (0.031)	0.00 (0.00)	-8.95 (0.037)	-7.52 (0.029)	-55.89 (0.452)	0.00 (0.00)
$\nu_3^{(\text{D7})}$	0.00 (0.00)	7.37 (0.007)	0.00 (0.00)	8.64 (0.007)	0.00 (0.00)	0.00 (0.00)	0.00 (0.00)	13.14 (0.054)
$(\nu_1 + \nu_1)^{(\text{D7})}$	-5.16 (0.042)	0.00 (0.00)	-9.19 (0.034)	0.00 (0.00)	-4.58 (0.000)	-1.94 (0.001)	-9.45 (0.024)	0.00 (0.00)
$\nu_4^{(\text{D7})}$	-4.44 (0.029)	0.00 (0.00)	-7.25 (0.021)	0.00 (0.00)	-1.82 (0.001)	7.97 (0.004)	-7.84 (0.010)	0.00 (0.00)
$(\nu_2 + \nu_2)^{(\text{D7})}$	-25.42 (0.304)	0.00 (0.00)	-55.79 (0.349)	0.00 (0.00)	-9.18 (0.015)	-8.10 (0.001)	-75.67 (0.090)	0.00 (0.00)
$(\nu_1 + \nu_2)^{(\text{D7})}$	0.00 (0.00)	-12.19 (0.072)	0.00 (0.133)	11.59 (0.037)	0.00 (0.00)	0.00 (0.00)	0.00 (0.00)	-21.72 (0.006)

TABLE VI. Tunneling matrix elements for the first 8 localized vibrational states of partially deuterated malonaldehyde. Values in parentheses correspond to the estimated error due to the neglect of the overlap term.

No.	$E^{(\text{pairs})}$	$E^{(4)}$	$E^{(8)}$
1	13974.27	13972.91	13971.48
2	14016.96	14015.52	14014.49
3	14296.86	14298.42	14286.79
4	14295.75	14295.44	14294.91
5	14314.69	14313.95	14313.54
6	14391.55	14392.78	14381.17
7	14383.28	14384.05	14383.32
8	14446.16	14446.45	14445.64
9	14540.00	-	14537.31
10	14549.82	-	14549.32
11	14541.38	-	14556.57
12	14560.53	-	14561.08
13	14597.33	-	14598.21
14	14596.99	-	14598.33
15	14641.54	-	14642.66
16	14696.90	-	14709.18

TABLE VII. Vibrational energy levels of partially deuterated malonaldehyde obtained from VCI energies of localized states either by splitting pairs of degenerate levels, or by diagonalizing model Hamiltonian constructed from 4 or 8 localized states in each minimum.

which gives  $\phi = 36.8^\circ$ . It thus appears that the inclusion of the additional interactions corrects the mixing angle towards the experimental value.

Changes in the vibrational levels of the excited states in the  $8 \times 8$  and the  $16 \times 16$  matrix model, listed in Table VII. are qualitatively similar to the case of homoisotopic malonaldehyde due to similarity in the TM elements. The vibrational tunneling spectrum is shown graphically in Figure 10. One significant difference here is that some doublet states change order of their components after the inclusion of additional vibrational states in the model due to their proximity in energy upon deuteration, as seen in Figure 10. Another difference is the absence of symme-

try in the wavefunctions with respect to the symmetry operation that connects the minima in the homoisotopic case. As a result, the extensions of the  $2 \times 2$  model to higher dimensionality matrix models will mix both, the lower and the higher components of a doublet, with all other doublets. Finally, due to the proximity of vibrational states, the lower components of the  $(\nu_1 + \nu_1)$ ,  $\nu_4$  and  $(\nu_2 + \nu_2)$  doublets are significantly mixed, as can be seen in Table VIII. This mixing between the states changes their energies, but it is also expected to affect the intensity of the transition to the 11<sup>th</sup> state as well, as its  $\nu_4$  component, in Table VIII, has a higher transition dipole moment, being the singly excited state.

#### IV. CONCLUSIONS

We applied a combination of VSCF/VCI and instanton theory to calculate vibrational tunneling spectra of some exemplary double-well systems in full dimensionality at a much reduced computational cost in comparison with the exact QM methods. The VSCF/VCI method was used to compute the single-well vibrational spectra, while the recently developed instanton method was used to determine the wavefunctions inside the barrier that separates the wells at a comparatively negligible computational cost. The interaction between the states of different wells was obtained from the Herring formula evaluated at the dividing surface inside the barrier. Herring formula was rederived in an  $N \times N$  matrix model ( $N > 2$ ) and the size of the associated leading error term was analysed.

The accuracy of our approach was first tested on a model 2D system. It was shown that the JFI method can be used to compute the tunneling matrix elements that connect states in inequivalent wells and have excitations in different normal modes. The energy levels

No.	Pairs	(8)
1	0.953   GS <sup>(D7)</sup> ⟩	0.946   GS <sup>(D7)</sup> ⟩
	0.303   GS <sup>(D9)</sup> ⟩	0.313   GS <sup>(D9)</sup> ⟩
2	-0.303   GS <sup>(D7)</sup> ⟩	-0.316   GS <sup>(D7)</sup> ⟩
	0.953   GS <sup>(D9)</sup> ⟩	0.946   GS <sup>(D9)</sup> ⟩
3	0.826   $\nu_2^{(D7)}$ ⟩	0.797   $\nu_2^{(D7)}$ ⟩
	0.564   $\nu_2^{(D9)}$ ⟩	0.560   $\nu_2^{(D9)}$ ⟩
4	0.919   $\nu_1^{(D7)}$ ⟩	0.914   $\nu_1^{(D7)}$ ⟩
	0.394   $\nu_1^{(D9)}$ ⟩	0.401   $\nu_1^{(D9)}$ ⟩
5	-0.394   $\nu_1^{(D7)}$ ⟩	-0.403   $\nu_1^{(D7)}$ ⟩
	0.919   $\nu_1^{(D9)}$ ⟩	0.909   $\nu_1^{(D9)}$ ⟩
6	-0.564   $\nu_2^{(D7)}$ ⟩	-0.573   $\nu_2^{(D7)}$ ⟩
	0.826   $\nu_2^{(D9)}$ ⟩	0.794   $\nu_2^{(D9)}$ ⟩
7	0.990   $\nu_3^{(D7)}$ ⟩	0.984   $\nu_3^{(D7)}$ ⟩
	-0.139   $\nu_3^{(D9)}$ ⟩	-0.138   $\nu_3^{(D9)}$ ⟩
8	0.139   $\nu_3^{(D7)}$ ⟩	0.138   $\nu_3^{(D7)}$ ⟩
	0.990   $\nu_3^{(D9)}$ ⟩	0.987   $\nu_3^{(D9)}$ ⟩
9	0.566   $(\nu_1 + \nu_1)^{(D7)}$ ⟩ 0.824   $(\nu_1 + \nu_1)^{(D9)}$ ⟩	0.505   $(\nu_1 + \nu_1)^{(D7)}$ ⟩
		0.293   $(\nu_2 + \nu_2)^{(D7)}$ ⟩
		0.761   $(\nu_1 + \nu_1)^{(D9)}$ ⟩
		-0.233   $(\nu_2 + \nu_2)^{(D9)}$ ⟩
10	0.824   $(\nu_1 + \nu_1)^{(D7)}$ ⟩	0.830   $(\nu_1 + \nu_1)^{(D7)}$ ⟩
	-0.566   $(\nu_1 + \nu_1)^{(D9)}$ ⟩	-0.543   $(\nu_1 + \nu_1)^{(D9)}$ ⟩
11	0.784   $(\nu_2 + \nu_2)^{(D7)}$ ⟩ 0.621   $(\nu_2 + \nu_2)^{(D9)}$ ⟩	0.354   $\nu_4^{(D7)}$ ⟩
		0.626   $(\nu_2 + \nu_2)^{(D7)}$ ⟩
		-0.349   $(\nu_1 + \nu_1)^{(D9)}$ ⟩
		0.537   $(\nu_2 + \nu_2)^{(D9)}$ ⟩
12	0.975   $\nu_4^{(D7)}$ ⟩ -0.222   $\nu_4^{(D9)}$ ⟩	0.895   $\nu_4^{(D7)}$ ⟩
		-0.299   $(\nu_2 + \nu_2)^{(D7)}$ ⟩
		-0.262   $\nu_4^{(D9)}$ ⟩
		-0.161   $(\nu_2 + \nu_2)^{(D9)}$ ⟩
13	0.222   $\nu_4^{(D7)}$ ⟩	0.236   $\nu_4^{(D7)}$ ⟩
	0.975   $\nu_4^{(D9)}$ ⟩	0.961   $\nu_4^{(D9)}$ ⟩
14	0.782   $(\nu_1 + \nu_2)^{(D7)}$ ⟩	0.778   $(\nu_1 + \nu_2)^{(D7)}$ ⟩
	0.624   $(\nu_1 + \nu_2)^{(D9)}$ ⟩	0.622   $(\nu_1 + \nu_2)^{(D9)}$ ⟩
15	-0.624   $(\nu_1 + \nu_2)^{(D7)}$ ⟩	-0.623   $(\nu_1 + \nu_2)^{(D7)}$ ⟩
	0.782   $(\nu_1 + \nu_2)^{(D9)}$ ⟩	0.780   $(\nu_1 + \nu_2)^{(D9)}$ ⟩
16	-0.621   $(\nu_2 + \nu_2)^{(D7)}$ ⟩	-0.612   $(\nu_2 + \nu_2)^{(D7)}$ ⟩
	0.784   $(\nu_2 + \nu_2)^{(D9)}$ ⟩	0.764   $(\nu_2 + \nu_2)^{(D9)}$ ⟩

TABLE VIII. Dominant configurations of vibrational states of partially deuterated malonaldehyde, computed either by splitting pairs of degenerate states or by diagonalizing model Hamiltonian constructed with 8 localized states in each minimum.

of the asymmetric system exhibit avoided crossings with the variation of the frequency or depth of one well relative to the other, which reproduces the exact QM results with high accuracy. The method was then tested on malonaldehyde in full dimensionality, where good agreement was achieved with the exact MCTDH result in the absolute energies and their splittings. It was shown that the extension of the standard  $2 \times 2$  model can influence the vibrational energies. Perhaps, one might argue that the results do not change dramatically in malonaldehyde, but it was shown that the model is able to accommodate the additional vibrational states in systems where they lie close in energy.

Finally, the method was used to calculate the vi-

brational spectrum of the low-lying states in partially deuterated malonaldehyde. This system would be at the limit of presently available exact quantum methods. The ground state mixing angle was compared to the experiment and the influence including additional vibrational states was shown to affect the angle and the order of some states in the spectrum.

The method is expected to perform well for mid-sized molecules, where rotational motion, which is neglected in this work, can be separated from the tunneling dynamics, and for moderately anharmonic systems with high barriers and, consequently, small tunneling splittings. It is exactly in these circumstances that the exact QM methods come at a prohibitive computational cost. The developed combined approach can be used to calculate the low-lying vibrational spectra in systems with arbitrary number of wells, which are not necessarily related by symmetry. This makes the method particularly suitable to studying of clusters, e.g., for the assignment of spectra in water clusters, which feature multiple minima and high barriers in their bifurcation dynamics (where hydrogen bonds are broken and reformed). The computational cost of our approach is concentrated in solving the single-well spectra separately. Instead of VSCF/VCI, other high-level methods can be employed if computational demands allow it. Future work will concentrate on including rotational motion in our approach<sup>36</sup> in an approximate manner.

#### Appendix A: Path invariance with respect to addition of switching function

We show below that the addition of a function  $f(S)$ , which only depends on the coordinate  $S$  along the path, to the potential,

$$\tilde{V}(\mathbf{x}) = V(\mathbf{x}) - f(S), \quad (\text{A1})$$

does not change the shape of the MAP, but only scales the imaginary time parameter  $\tau$ . The statement is valid if the function  $f$  does not change the position or shape of the minima, i.e., it satisfies

$$\begin{aligned} \lim_{S \rightarrow 0(S_{\text{tot}})} f(S) &= 0, \\ \lim_{S \rightarrow 0(S_{\text{tot}})} f'(S) &= 0, \\ \lim_{S \rightarrow 0(S_{\text{tot}})} f''(S) &= 0, \end{aligned} \quad (\text{A2})$$

and is negligible in comparison with the potential in the region between the minima,  $f(S) \ll V(S)$ .

Path  $\mathbf{x}(\tau)$  is the characteristic for potential  $V$  and it satisfies

$$\begin{aligned} \frac{d^2}{d\tau^2} \mathbf{x}(\tau) &= \nabla V, \\ \frac{dS}{d\tau} &= p_0 = \sqrt{2V}, \end{aligned} \quad (\text{A3})$$



where  $S$  is the arc length distance along the path. We define the scaled imaginary time as

$$d\tilde{\tau} = \frac{d\tau}{\sqrt{1 - \frac{f(S)}{V}}}. \quad (\text{A4})$$

The scaled momentum then becomes

$$\tilde{p}_0 = \frac{dS}{d\tilde{\tau}} = \sqrt{2(V - f(S))} = \sqrt{2\tilde{V}}. \quad (\text{A5})$$

The momentum vector transforms as

$$\begin{aligned} \frac{d}{d\tilde{\tau}} \mathbf{x}(\tilde{\tau}) &= \frac{d\mathbf{x}}{d\tau} \sqrt{1 - \frac{f(S)}{V}}, \\ \tilde{\mathbf{p}}_0 &= \mathbf{p}_0 \sqrt{1 - \frac{f(S)}{V}}, \end{aligned} \quad (\text{A6})$$

whereas the acceleration becomes

$$\begin{aligned} \frac{d^2}{d\tilde{\tau}^2} \mathbf{x}(\tilde{\tau}) &= \nabla(V - f(S)) + \frac{f(S)}{V} \left( \frac{\mathbf{p}_0}{p_0} \frac{d}{dS} V - \nabla V \right), \\ \frac{d^2}{d\tilde{\tau}^2} \mathbf{x}(\tilde{\tau}) &= \nabla(\tilde{V}) - \frac{f(S)}{V} (\nabla V)_\perp, \end{aligned} \quad (\text{A7})$$

where the symbol  $\perp$  in the subscript denotes the component of the vector that is perpendicular to the path. Now, if the function  $f(S)$  satisfies the conditions in Eq. (A2) and is significantly smaller than the potential, the second term on the right hand side of Eq. (A7) is small everywhere on the path in comparison to the gradient of the potential. It can therefore be ignored, and the obtained equation takes the form of the equation for the characteristic but on the modified potential.

## Appendix B: Dependence of tunneling matrix elements with respect to the position of the dividing plane

TM elements between the states with, at most, one excitation ( $\nu = 0 - 1$  and  $\nu' = 0 - 1$ ) can be expressed as

$$\begin{aligned} h_{\nu\nu'} &= \sqrt{\frac{\sqrt{\det' \mathbf{A}_0^{(L)} \det' \mathbf{A}_0^{(R)}} p_0^{(L)} + p_0^{(R)}}{\pi \det' \tilde{\mathbf{A}}} \frac{p_0^{(L)} + p_0^{(R)}}{2}} \\ &\times \left( F^{(L)} \right)^\nu \left( F^{(R)} \right)^{\nu'} \sqrt{\frac{\left( 2\omega_e^{(L)} \right)^\nu \left( 2\omega_e^{(R)} \right)^{\nu'}}{(2\nu - 1)!! (2\nu' - 1)!!}} \\ &\times e^{-\int_0^{S_{cp}} p_0^{(L)} dS - \int_{S_{cp}}^{S_{tot}} p_0^{(R)} dS} \\ &\times e^{-\frac{1}{2} \int_0^{S_{cp}} \frac{\text{Tr}(\mathbf{A}^{(L)} - \mathbf{A}_0^{(L)})}{p_0^{(L)}} dS - \frac{1}{2} \int_{S_{cp}}^{S_{tot}} \frac{\text{Tr}(\mathbf{A}^{(R)} - \mathbf{A}_0^{(R)})}{p_0^{(R)}} dS}, \end{aligned} \quad (\text{B1})$$

where the contribution of  $\mathbf{U}$  terms has been neglected (see Eq. (9)). It is known that, unless these terms exclusively contribute to the TM elements, they introduce the dependence of the TM element  $h_{\nu\nu'}$  on the connection

point, as shown previously<sup>42</sup>. Therefore, we omit them in this treatment to separate the effect of  $\mathbf{U}$  terms from the effect of asymmetry on the connection point  $S_{cp}$ . The case of multiple excitations, as well as that of the  $\mathbf{U}$  terms can be derived in analogous fashion.

Dependence on the position of the connection point can be determined by differentiating the TM element in Eq. (B1) with respect to  $S_{cp}$ . Small changes in the connection point correspond to the addition of function  $f(S)$  of the following form

$$f(S) = \begin{cases} -d & S_{cp} - \varepsilon < S < S_{cp} \\ +d & S_{cp} < S < S_{cp} + \varepsilon \\ 0 & \text{elsewhere} \end{cases} \quad (\text{B2})$$

to the potential in the action integral, where  $\varepsilon$  denotes the change in the connection point. As discussed in Appendix A, the addition of  $f$  does not change the shape of the path. The differentiation can thus be performed on the same path. Furthermore, if the connection point is located deep inside the barrier, we can approximate

$$p_0^{(L)} \approx p_0^{(R)} = \bar{p}_0. \quad (\text{B3})$$

Following the differentiation, as described in Ref. 42, we obtain

$$\begin{aligned} \frac{d}{dS_{cp}} h_{\nu\nu'} &= \frac{h_{\nu\nu'}}{\bar{p}_0} \left[ 2 \frac{d\bar{p}_0}{dS_{cp}} + \omega_e^{(L)} \delta_{\nu,1} - \omega_e^{(R)} \delta_{\nu',1} + \right. \\ &\quad \left. \bar{p}_0 (p_0^{(R)} - (p_0^{(L)})^2) + \frac{1}{2} \text{Tr} \left( \mathbf{A}_\perp^{(L)} - \mathbf{A}_\perp^{(R)} \right) - \right. \\ &\quad \left. \frac{1}{2} \text{Tr} \left( \mathbf{A}^{(L)} - \mathbf{A}^{(R)} \right) + \frac{1}{2} \text{Tr} \left( \mathbf{A}_0^{(L)} - \mathbf{A}_0^{(R)} \right) \right] \\ \frac{d}{dS_{cp}} h_{\nu\nu'} &= \frac{h_{\nu\nu'}}{\bar{p}_0} \left[ \omega_e^{(L)} \delta_{\nu,1} - \omega_e^{(R)} \delta_{\nu',1} + \right. \\ &\quad \left. \frac{1}{2} \left( p_0^{(R)2} - p_0^{(L)2} \right) + \frac{1}{2} \text{Tr} \left( \mathbf{A}_0^{(L)} - \mathbf{A}_0^{(R)} \right) \right] \\ \frac{d}{dS_{cp}} h_{\nu\nu'} &= \frac{h_{\nu\nu'}}{\bar{p}_0} \left[ \omega_e^{(L)} \delta_{\nu,1} + \frac{1}{2} \text{Tr} \mathbf{A}_0^{(L)} - \omega_e^{(R)} \delta_{\nu',1} \right. \\ &\quad \left. - d - \frac{1}{2} \text{Tr} \mathbf{A}_0^{(R)} \right] \\ \frac{d}{dS_{cp}} h_{\nu\nu'} &= \frac{h_{\nu\nu'}}{\bar{p}_0} \left( E^{(L)} - E^{(R)} \right), \end{aligned} \quad (\text{B4})$$

where  $E^{(L/R)}$  denote the energies of the local L/R wavefunctions and  $\mathbf{A}_\perp$  is the matrix  $\mathbf{A}$  projected onto the space orthogonal to the MAP. From Eq. (B4), it is evident that the TM element will only be invariant with respect to variation in  $S_{cp}$  if the two local L/R states are in resonance. Otherwise, the TM element depends on the position of the connection point and the dependence is stronger for larger mismatch in the local energies.

The dependence on the connection point can be traced to the neglected integral in the derivation of Herring formula in Eq. (3) involving  $\phi_\nu^{(L)} \phi_{\nu'}^{(R)}$  term. Inclusion of this

term, transforms the formula for the TM element into

$$\tilde{h}_{\nu\nu'} = \frac{1}{2} \int \left( \phi_{\nu'}^{(R)} \frac{\partial}{\partial S} \phi_{\nu}^{(L)} - \phi_{\nu}^{(L)} \frac{\partial}{\partial S} \phi_{\nu'}^{(R)} \right) \delta(f(\mathbf{x})) d\mathbf{x} + (E^{(L)} - E^{(R)}) \int_L \phi_{\nu}^{(L)} \phi_{\nu'}^{(R)} d\mathbf{x}, \quad (\text{B5})$$

where the second integral is taken over the space on the ‘left’ side of the dividing plane. We then differentiate the extended expression, Eq. (B5), with respect to  $S_{cp}$ , and observe that the derivative of the additional term in Eq. (B5) is the integral over the dividing plane. The derivative of the TM element becomes

$$\frac{\partial}{\partial S_{cp}} \tilde{h}_{\nu\nu'} = (E^{(L)} - E^{(R)}) \frac{h_{\nu\nu'}}{\bar{p}_0} + (E^{(L)} - E^{(R)}) \int \phi_{\nu}^{(L)} \phi_{\nu'}^{(R)} \delta(f(\mathbf{x})) d\mathbf{x}, \quad (\text{B6})$$

where use has been made of Eq. (B4). We note now that the surface integral in Eq. (B6) differs from the ‘old version’ of  $h_{\nu\nu'}$  only by the momentum term  $\bar{p}_0$ . However, this factor is taken to be constant on the dividing plane and it can be taken out of the integral, which leads to

$$\frac{\partial}{\partial S_{cp}} \tilde{h}_{\nu\nu'} = (E^{(L)} - E^{(R)}) \frac{h_{\nu\nu'}}{\bar{p}_0} - (E^{(L)} - E^{(R)}) \frac{h_{\nu\nu'}}{\bar{p}_0} = 0. \quad (\text{B7})$$

While it would seem obvious to use the instanton wavefunctions in Eq. (6) and compute the additional term that arises in Eq. (B6) in order to eliminate the dependence on  $S_{cp}$ , the semiclassical approximation breaks down beyond the barrier and would lead to a divergence of the integral. We are thus left with no option but to neglect the term and treat it as an error term in the TM element.

We tried to estimate the error term, introduced above, by calculating the overlap of the harmonic oscillator wavefunctions centered at the two minima. The overlap is obtained following the method of Ref. 64, where Frank-Condon factors between the shifted harmonic oscillators are computed. The calculation requires the knowledge of molecular geometries and harmonic frequencies in the two minima and does not add to the overall computational cost. The errors for the partially deuterated malonaldehyde were found to be small and are listed in the parenthesis in Table VI. We found that it was safe to neglect the error terms unless the connection point is moved far from the position of the barrier top, or unless the energy difference between the two states is large in relation to the barrier height. Moreover, we note that as the energy difference increases, the contribution of the TM element to the energy level decreases, as seen from the second-order perturbation treatment,

$$E_i^{(L),(2)} = \sum_j \frac{h_{ij}^2}{E_i^{(L)} - E_j^{(R)}} \\ E_i^{(R),(2)} = \sum_j \frac{h_{ji}^2}{E_i^{(R)} - E_j^{(L)}}. \quad (\text{B8})$$

Since  $h_{ij}$  are expected to be small in the deep tunneling regime, the contributions of the states that lie far from the resonance quickly approach zero. Thus, even for larger energy differences, the computed energy levels remain stable.

Dependence of the tunneling matrix elements on the position of the dividing plane was also tested by moving the dividing plane from  $0.25S_{\text{tot}}$  to  $0.75S_{\text{tot}}$ , where  $S_{\text{tot}}$  is the MAP length. All the matrix elements displayed monotonous dependence on  $S_{cp}$ , with an inflection point located near the position of the barrier top, and a region of relative stability around it. As the dividing plane is moved away from the barrier top, the TM elements begin to change significantly. These TM elements connect the states with a significant disparity in their local energies. For example, the TM elements between the  $(\nu_2 + \nu_2)$  state and the GS or the  $\nu_2$ -excited state change from  $-11 \text{ cm}^{-1}$  to  $-55 \text{ cm}^{-1}$  and from  $-36 \text{ cm}^{-1}$  to  $-80 \text{ cm}^{-1}$ , respectively. However, a large energy difference between the involved states also implies that the TM elements do not profoundly affect the overall energy. The GS TS varies by  $\approx 7 \text{ cm}^{-1}$  in this region. If we limit ourselves to the region between  $0.40S_{\text{tot}}$  and  $0.60S_{\text{tot}}$ , the variation of the GS TS is only  $1.5 \text{ cm}^{-1}$ , which is within the error of the VCI method used to compute the local energies. Similar errors are observed for the other energy levels. The method can thus give reliable results when the dividing plane is placed in the vicinity of the barrier top.

### Appendix C: Vibrational self consistent field (VSCF) and vibrational configuration interaction (VCI)

The idea behind the VSCF approach is to approximate the vibrational wavefunction by a Hartree product of single-mode (1M) functions as

$$\psi(\mathbf{q}) = \phi_0^{(1)}(q_1) \dots \phi_0^{(N)}(q_N), \quad (\text{C1})$$

where  $q_i$  is the  $i$ -th normal mode coordinate. The above form can efficiently be employed in combination with the  $n$ -mode representation<sup>59</sup> of the potential

$$V(\mathbf{q}) = V_{\text{min}} + \sum_{i=1}^N V_i^{(1M)}(q_i) + \sum_{i=1}^{N-1} \sum_{j=i}^N V_{ij}^{(2M)}(q_i, q_j) + \dots \quad (\text{C2})$$

In this paper, the expansion was truncated at the two-mode (2M) terms. Using wavefunction in Eq. (C1) and variational principle, it can be shown that the optimal 1M functions satisfy a set of coupled 1M equations

$$\frac{1}{2} \frac{d^2}{dq_i^2} \phi^{(i)}(q_i) + (V_{\text{min}} + V_i^{(1M)}(q_i) + \sum_{\substack{j=1 \\ j \neq i}}^{N_{\text{dof}}} \langle \phi_0^{(j)}(q_j) | V_{ij}^{(2M)}(q_i, q_j) | \phi_0^{(j)}(q_j) \rangle) \phi^{(i)}(q_i) = \varepsilon_i \phi^{(i)}(q_i), \quad (\text{C3})$$

which can be solved via an SCF algorithm. The 1M functions  $\phi_0^i$  are expanded in a basis set  $\{\chi_j^{(i)}\}$ . In this paper, the lowest  $N_{\text{basis}}$  states of the harmonic oscillator (HO) are used. The 1M and 2M potential energy terms in Eq. (C2) are fitted to polynomials of order  $N_{\text{fit}}$

$$V_i^{(1M)}(q_i) = \sum_{j=2}^{N_{\text{fit}}} C_j^{(i)} q_i^j$$

$$V_{ij}^{(2M)}(q_i, q_j) = \sum_{k=1}^{N_{\text{fit}}-1} \sum_{l=1}^{N_{\text{fit}}-k} C_{kl}^{(ij)} q_i^k q_j^l. \quad (\text{C4})$$

These choices enable us to compute the potential matrix elements exactly. For that purpose, we calculate the matrices  $\mathbf{Q}_i^{(j)}$ , the representations of operators  $q_i^j$  in the HO basis. This can be done recursively using ladder operators

$$\begin{aligned} \langle \chi_j^{(i)} | q_i^n | \chi_k^{(i)} \rangle &= \frac{1}{\sqrt{2\omega_i}} \langle \chi_j^{(i)} | q_i^{n-1} (\hat{a}_i + \hat{a}_i^\dagger) | \chi_k^{(i)} \rangle = \\ &= \sqrt{\frac{k}{2\omega_i}} \langle \chi_j^{(i)} | q_i^{n-1} | \chi_{k-1}^{(i)} \rangle + \sqrt{\frac{k+1}{2\omega_i}} \langle \chi_j^{(i)} | q_i^{n-1} | \chi_{k+1}^{(i)} \rangle. \end{aligned} \quad (\text{C5})$$

The matrices  $\mathbf{Q}_i^{(j)}$  are then stored and the SCF algorithm is started using the initial guess  $\phi_0^{(i)} = \chi_0^{(i)}$ . The effective Hamiltonian in Eq. (C3) is constructed for each mode in the HO basis, diagonalized and the obtained 1M functions corresponding to the lowest eigenvalue taken as new  $\phi_0^{(i)}$ . Once VSCF has converged, the obtained virtual 1M functions can be used to construct the VCI Hamiltonian

$$H_{IJ} = \langle \phi_{i_1}^{(1)} \dots \phi_{i_N}^{(N)} | \hat{H} | \phi_{j_1}^{(1)} \dots \phi_{j_N}^{(N)} \rangle. \quad (\text{C6})$$

The matrix elements of  $H_{IJ}$  are computed using  $\mathbf{Q}_i^{(j)}$  matrices and the coefficients of 1M functions in the HO basis. Its eigenvalues represent the VCI energies, while the eigenvectors can be used to determine the dominant configuration  $\phi_{i_1}^{(1)} \dots \phi_{i_N}^{(N)}$  and learn which normal modes are excited in the particular state.

<sup>1</sup>R. P. Bell, *The Tunnel Effect in Chemistry* (Chapman and Hall, London, 1980).

<sup>2</sup>F. Hund, Z. Phys. **43**, 805 (1927).

<sup>3</sup>V. A. Benderskii, D. E. Makarov, and C. A. Wight, *Chemical Dynamics at Low Temperatures*, Adv. Chem. Phys., Vol. 88 (Wiley, New York, 1994).

<sup>4</sup>Š. Urban, V. Špirko, D. Papoušek, J. Kauppinen, S. Belov, L. Gershtein, and A. Krupnov, J. Mol. Spectrosc. **88**, 274 (1981).

<sup>5</sup>D. W. Firth, K. Beyer, M. A. Dvorak, S. W. Reeve, A. Grushow, and K. R. Leopold, J. Chem. Phys. **94**, 1812 (1991).

<sup>6</sup>E. T. Mengesha, J. Sepiol, P. Borowicz, and J. Waluk, J. Chem. Phys. **138**, 174201 (2013).

<sup>7</sup>K. Tanaka, M. Toshimitsu, K. Harada, and T. Tanaka, J. Chem. Phys. **120**, 3604 (2004).

<sup>8</sup>M. T. Cvitaš and J. O. Richardson, in *Molecular Spectroscopy and Quantum Dynamics*, edited by R. Marquardt and M. Quack (Elsevier, 2020) Chap. 9, pp. 301–326.

<sup>9</sup>E. Jahr, G. Laude, and J. O. Richardson, J. Chem. Phys. **153**, 094101 (2020).

<sup>10</sup>S. L. Baughcum, R. W. Duerst, W. F. Rowe, Z. Smith, and E. B. Wilson, J. Am. Chem. Soc. **103**, 6296 (1981).

<sup>11</sup>D. H. Zhang, Q. Wu, J. Z. H. Zhang, M. von Dirke, and Z. Bačić, J. Chem. Phys. **102**, 2315 (1995).

<sup>12</sup>J. Šmydke, C. Fábri, J. Sarka, and A. G. Császár, Phys. Chem. Chem. Phys. **21**, 3453 (2019).

<sup>13</sup>K. Liu, M. G. Brown, M. R. Viant, J. D. Cruzan, and R. J. Saykally, Mol. Phys. **89**, 1373 (1996).

<sup>14</sup>M. Eraković and M. T. Cvitaš, Phys. Chem. Chem. Phys. **23**, 4240 (2021).

<sup>15</sup>L. González, O. Mó, and M. Yáñez, J. Phys. Chem. A **101**, 9710 (1997).

<sup>16</sup>V. E. Bondybey, R. C. Haddon, and P. M. Rentzepis, J. Am. Chem. Soc. **106**, 5969 (1984).

<sup>17</sup>A. Oppenländer, C. Rambaud, H. P. Trommsdorff, and J.-C. Vial, Phys. Rev. Lett. **63**, 1432 (1989).

<sup>18</sup>B. V. Hall, S. Whitlock, R. Anderson, P. Hannaford, and A. I. Sidorov, Phys. Rev. Lett. **98**, 030402 (2007).

<sup>19</sup>S. Takahashi, I. S. Tupitsyn, J. van Tol, C. C. Beedle, D. N. Hendrickson, and P. C. E. Stamp, Nature **476**, 76 (2011).

<sup>20</sup>P. R. Johnson, W. T. Parsons, F. W. Strauch, J. R. Anderson, A. J. Dragt, C. J. Lobb, and F. C. Wellstood, Phys. Rev. Lett. **94**, 187004 (2005).

<sup>21</sup>P. M. Felker and Z. Bačić, J. Chem. Phys. **151**, 024305 (2019).

<sup>22</sup>M. Schröder and H.-D. Meyer, J. Chem. Phys. **141**, 034116 (2014).

<sup>23</sup>T. Hammer and U. Manthe, The Journal of Chemical Physics **136**, 054105 (2012).

<sup>24</sup>C. Leforestier, K. Szalewicz, and A. van der Avoird, J. Chem. Phys. **137**, 014305 (2012).

<sup>25</sup>C. L. Vaillant, D. J. Wales, and S. C. Althorpe, J. Chem. Phys. **148**, 234102 (2018).

<sup>26</sup>C. L. Vaillant, D. J. Wales, and S. C. Althorpe, J. Phys. Chem. Lett. **10**, 7300 (2019).

<sup>27</sup>V. Benderskii, E. Vetoshkin, S. Grebenshchikov, L. von Laue, and H. Trommsdorff, Chem. Phys. **219**, 119 (1997).

<sup>28</sup>Z. Smedarchina, W. Siebrand, and A. Fernández-Ramos, J. Chem. Phys. **137**, 224105 (2012).

<sup>29</sup>J. O. Richardson and S. C. Althorpe, J. Chem. Phys. **134**, 054109 (2011).

<sup>30</sup>G. V. Mil'nikov and H. Nakamura, J. Chem. Phys. **115**, 6881 (2001).

<sup>31</sup>M. Eraković, C. L. Vaillant, and M. T. Cvitaš, J. Chem. Phys. **152**, 084111 (2020).

<sup>32</sup>M. T. Cvitaš and S. C. Althorpe, J. Chem. Theory Comput. **12**, 787 (2016).

<sup>33</sup>M. T. Cvitaš, J. Chem. Theory Comput. **14**, 1487 (2018).

<sup>34</sup>G. V. Mil'nikov, T. Ishida, and H. Nakamura, J. Phys. Chem. A **110**, 5430 (2006).

<sup>35</sup>G. Mil'nikov, O. Kühn, and H. Nakamura, J. Chem. Phys. **123**, 074308 (2005).

<sup>36</sup>C. Vaillant and M. T. Cvitaš, Phys. Chem. Chem. Phys. **20**, 26809 (2018).

<sup>37</sup>E. Zwart, J. J. ter Meulen, W. L. Meerts, and L. H. Coudert, J. Mol. Spectrosc. **147**, 27 (1991).

<sup>38</sup>F. N. Keutsch, J. D. Cruzan, and R. J. Saykally, Chem. Rev. **103**, 2533 (2003).

<sup>39</sup>J. O. Richardson, C. Pérez, S. Lobsiger, A. A. Reid, B. Temelso, G. C. Shields, Z. Kisiel, D. J. Wales, B. H. Pate, and S. C. Althorpe, Science **351**, 1310 (2016).

<sup>40</sup>J. O. Richardson, D. J. Wales, S. C. Althorpe, R. P. McLaughlin, M. R. Viant, O. Shih, and R. J. Saykally, J. Phys. Chem. A **117**, 6960 (2013).

<sup>41</sup>M. T. Cvitaš and J. O. Richardson, Phys. Chem. Chem. Phys. **22**, 1035 (2019).

<sup>42</sup>M. Eraković and M. T. Cvitaš, J. Chem. Phys. **153** (2020), 10.1063/5.0024210.

- <sup>43</sup>G. V. Mil'nikov and H. Nakamura, J. Chem. Phys. **122**, 124311 (2005).
- <sup>44</sup>A. Garg, Am. J. Phys. **68**, 430 (2000).
- <sup>45</sup>C. Herring, Rev. Mod. Phys. **34**, 631 (1962).
- <sup>46</sup>F. Cesi, G. C. Rossi, and M. Testa, Ann. Phys. **206**, 318 (1991).
- <sup>47</sup>D. Mugnai and A. Ranfagni, Phys. Lett. A **109**, 219 (1985).
- <sup>48</sup>A. J. Leggett, S. Chakravarty, A. T. Dorsey, M. P. A. Fisher, A. Garg, and W. Zwerger, Rev. Mod. Phys. **59**, 1 (1987).
- <sup>49</sup>H. Dekker, Physica A **146**, 375 (1987).
- <sup>50</sup>D.-Y. Song, Ann. Phys. **323**, 2991 (2008).
- <sup>51</sup>D.-Y. Song, Ann. Phys. **362**, 609 (2015).
- <sup>52</sup>A. J. L. Seyyed M.H. Halataei, arXiv preprint arXiv:1703.05758 (2017).
- <sup>53</sup>W. Siebrand, Z. Smedarchina, and A. Fernández-Ramos, J. Chem. Phys. **139**, 021101 (2013).
- <sup>54</sup>V. Benderskii, E. Vetoshkin, and H. Trommsdorff, Chem. Phys. **244**, 299 (1999).
- <sup>55</sup>V. Benderskii, E. Vetoshkin, I. Irgibaeva, and H. Trommsdorff, Chem. Phys. **262**, 393 (2000).
- <sup>56</sup>S. Carter, J. M. Bowman, and N. C. Handy, Theor. Chim. Acta **100**, 191 (1998).
- <sup>57</sup>K. M. Christoffel and J. M. Bowman, Chem. Phys. Lett. **85**, 220 (1982).
- <sup>58</sup>J. M. Bowman, K. Christoffel, and F. Tobin, J. Phys. Chem. **83**, 905 (1979).
- <sup>59</sup>J. M. Bowman, S. Carter, and X. Huang, Int. Rev. Phys. Chem. **22**, 533 (2003).
- <sup>60</sup>G. Rauhut, J. Chem. Phys. **121**, 9313 (2004).
- <sup>61</sup>Y. Wang, B. J. Braams, J. M. Bowman, S. Carter, and D. P. Tew, J. Chem. Phys. **128**, 224314 (2008).
- <sup>62</sup>D. Ferro-Costas and A. Fernández-Ramos, in *Tunnelling in Molecules: Nuclear Quantum Effects from Bio to Physical Chemistry*, edited by J. Kästner and S. Kozuch (Royal Society of Chemistry, 2020) Chap. 9, pp. 283–327.
- <sup>63</sup>N. O. Lüttschwager, T. N. Wassermann, S. Coussan, and M. A. Suhm, Mol. Phys. **111**, 2211 (2013).
- <sup>64</sup>R. Berger, C. Fischer, and M. Klessinger, J. Phys. Chem. A **102**, 7157 (1998).



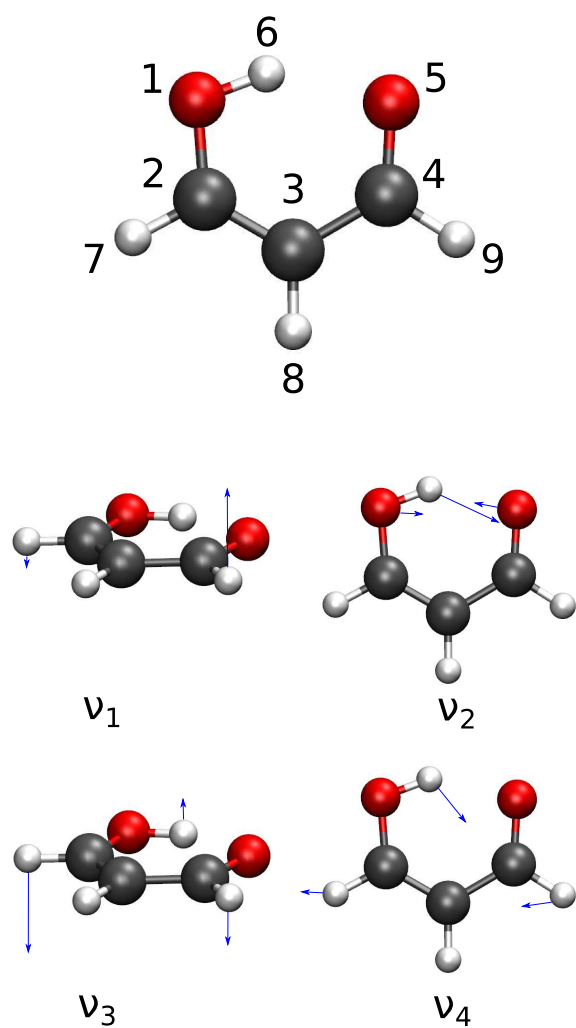


FIG. 3. Atom numbering and normal modes of malonaldehyde.

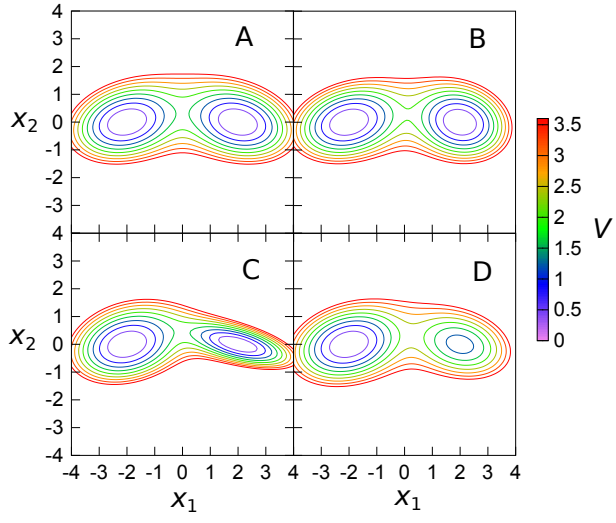


FIG. 4. Potential energy surfaces for model potential in Eq. (10) A) symmetric potential B) different  $\omega_1$  frequencies C) different  $\omega_2$  frequencies D)  $d > 0$   $d$ .

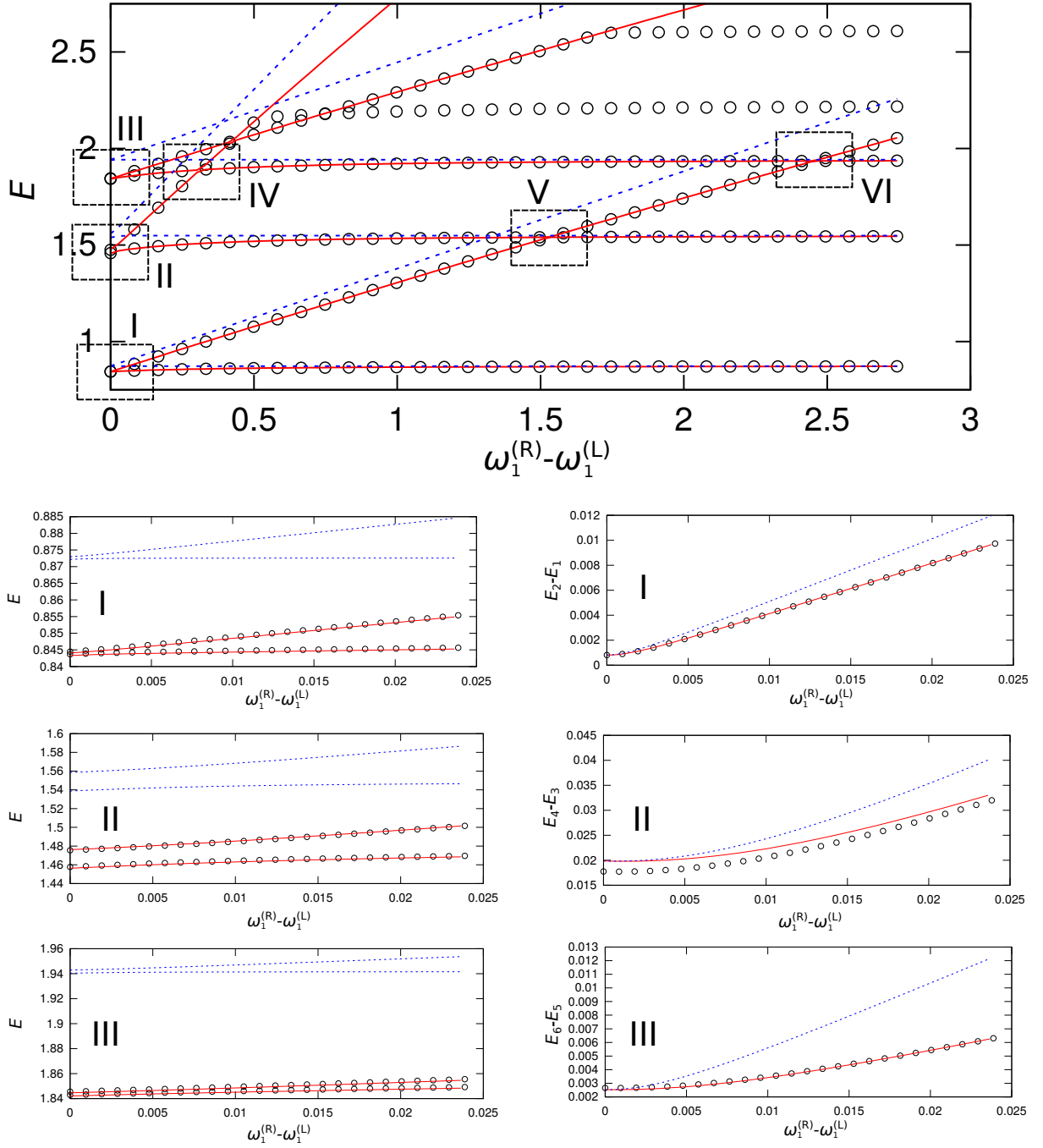


FIG. 5. Vibrational energies of first 6 states in double-well potential described with Eq. (10) for different values of  $\omega_1^{(R)}$ . Circles represent quantum-mechanical values, blue lines are obtained using instanton method with harmonic energies, red lines are obtained using instanton method with VCI energies.

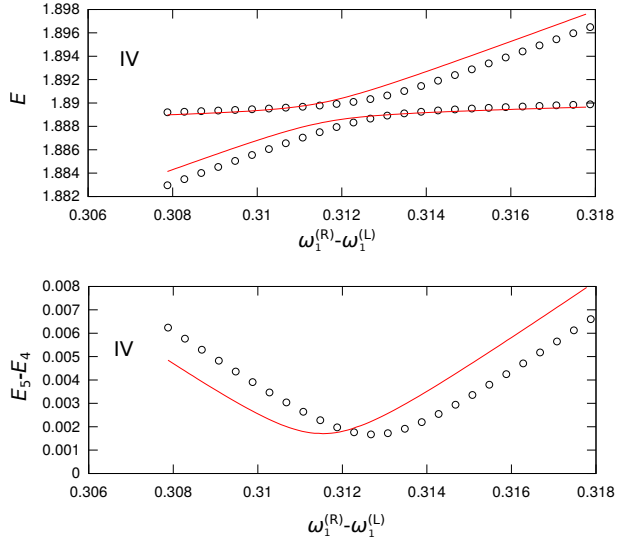


FIG. 6. Vibrational energies and their difference in the region of the avoided crossing between the first excited state in the right minimum and the second excited state in the left minimum. Circles represent quantum-mechanical values, while red lines represent values obtained using instanton method with VCI localized energies.



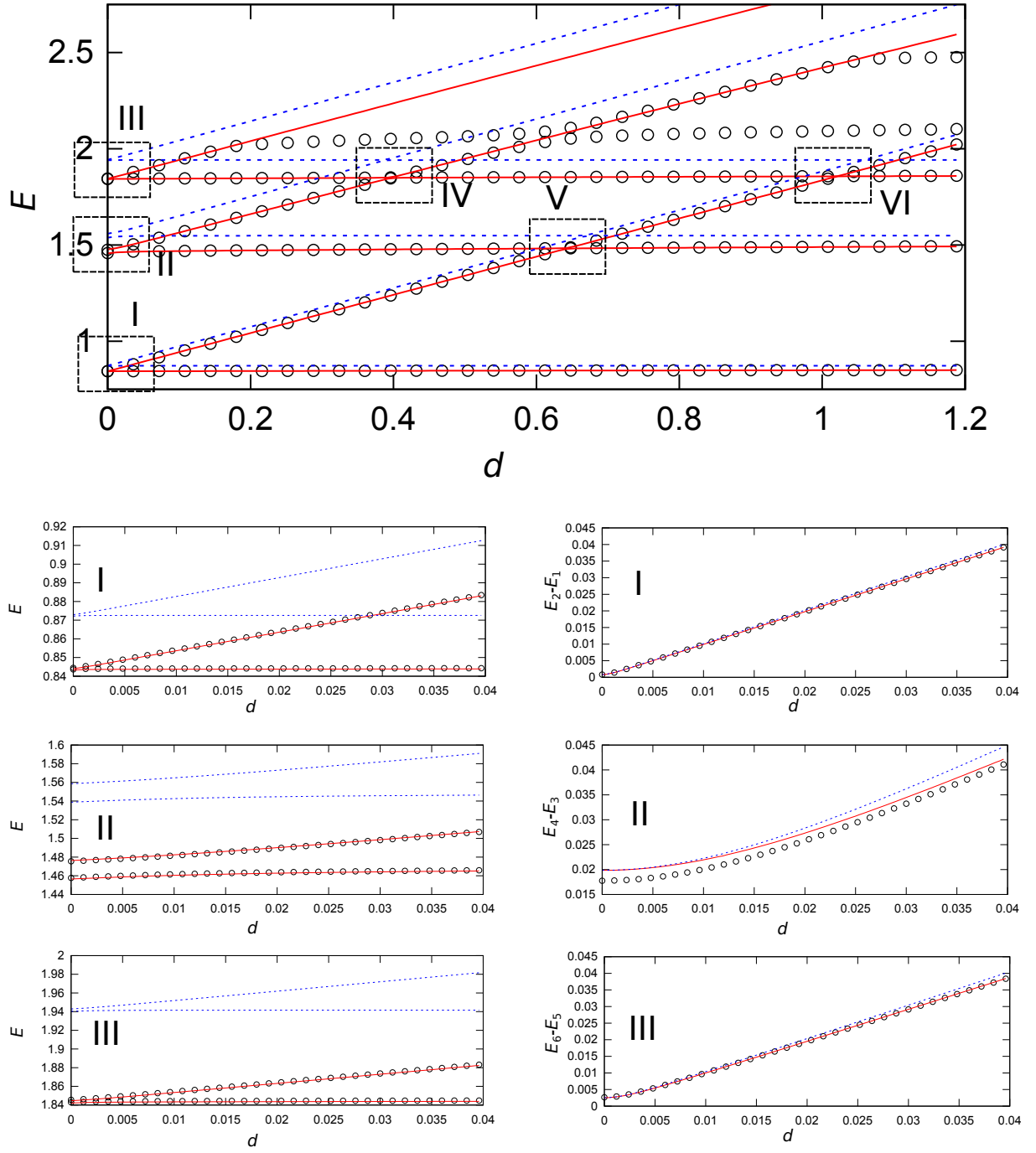


FIG. 7. Vibrational energies of first 6 states in double-well potential described with Eq. (10) for different values of  $d$ . Circles represent quantum-mechanical values, blue lines are obtained using instanton method with harmonic energies, red lines are obtained using instanton method with VCI energies.

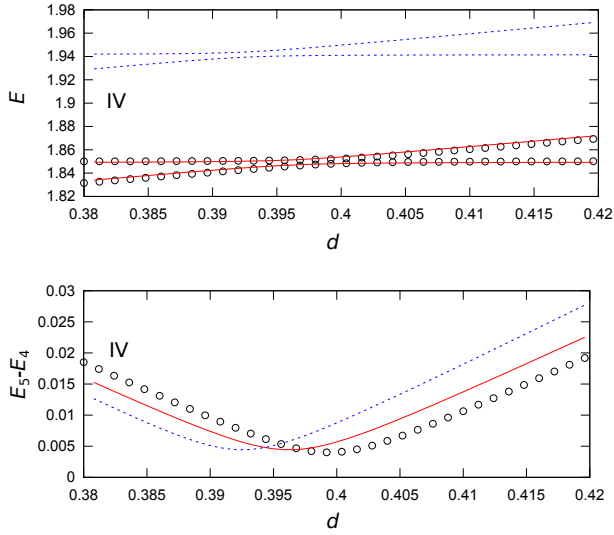


FIG. 8. Vibrational energies and their difference in the region of the avoided crossing between the first excited state in the right minimum and the second excited state in the left minimum. Circles represent quantum-mechanical values, while red lines represent values obtained using instanton method with VCI localized energies.

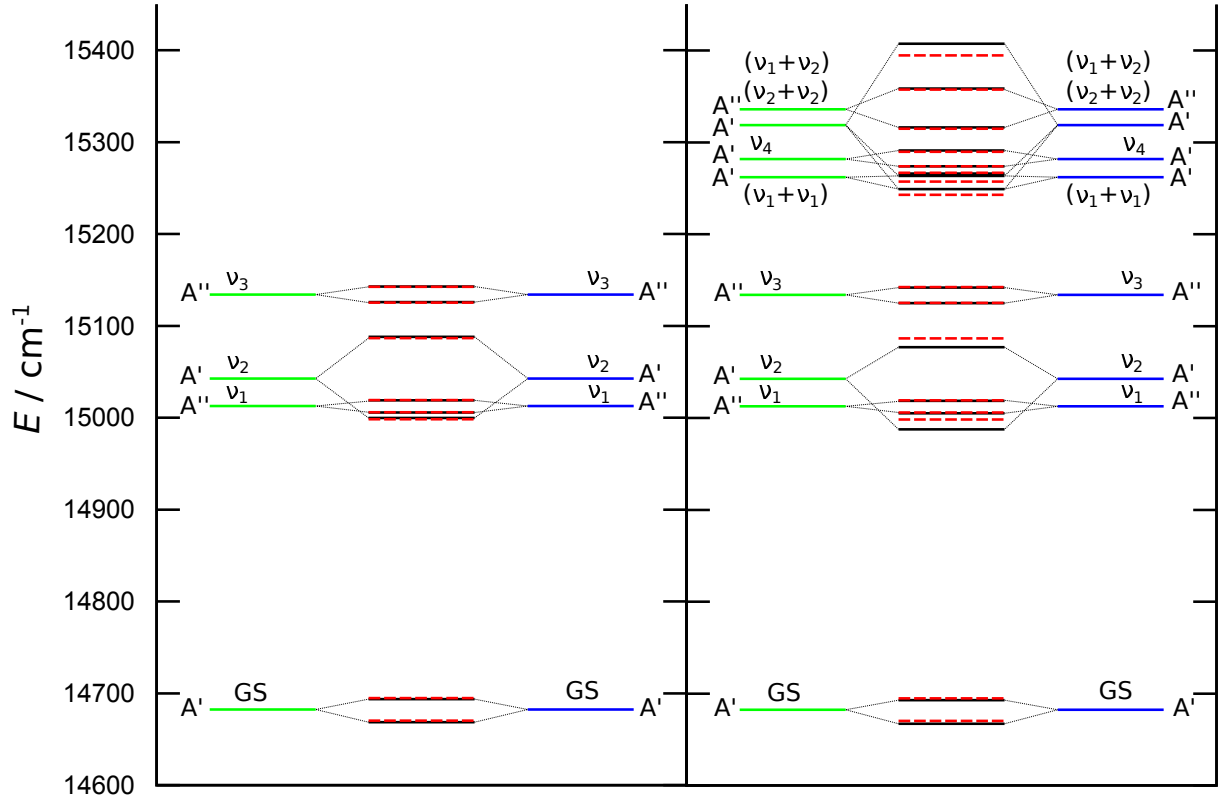


FIG. 9. Vibrational energies of first 16 states of malonaldehyde. Green and blue lines correspond to energies of localized wavefunctions, obtained using VCI approach, dashed red lines correspond to total energies obtained by including splittings of pairs of localized states, black lines correspond to total energies obtained from Hamiltonian matrix Eq. (1).

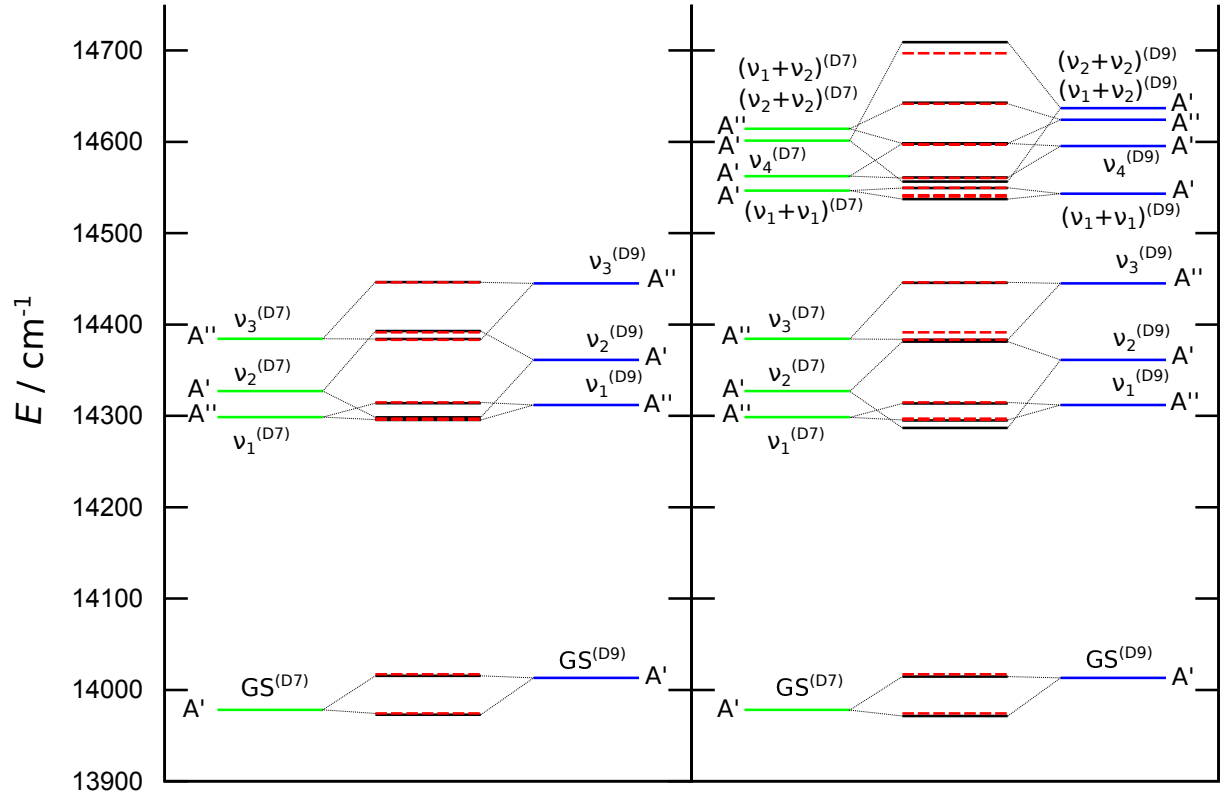


FIG. 10. Vibrational energies of first 16 states of partially deuterated malonaldehyde. Green and blue lines correspond to energies of localized wavefunctions, obtained using VCI approach, dashed red lines correspond to total energies obtained by including splittings of pairs of localized states, black lines correspond to total energies obtained from Hamiltonian matrix Eq. (1).